GEOSURV II UNINHABITED AERIAL VEHICLE

FINAL REPORT

PART B

AERODYNAMICS AND PROPULSION

Group Members

S. Clifford
T. McQueen
A. Janus
G. Blouin

Lead Engineer

J. Etele

April 2009

Page intentionally left blank

ABSTRACT

This document summarizes the work accomplished in 2008/2009 by the Aerodynamics and Propulsion group on the GeoSurv II UAV project. Progress was made towards a number of key project objectives. The engine was started and broken-in. Throttle and choke controls were designed and built for use on the prototype. The fuel system design was modified for the prototype and installed in the fuselage. An air data boom was designed, manufactured and tested for use on the prototype. A drag reduction study was undertaken using Computational Fluid Dynamics (CFD), focussing on redesign of the nose cone. A mount for the wind tunnel model was designed and manufactured. After failure of the wind tunnel model, it was repaired with new materials and successful wind tunnel tests were performed. An analysis of the aircraft performance during take-off was performed and the dynamic simulation was further developed from a linear model to a non-linear model.

A number of recommendations are made for future project teams to continue the work thus far. Among the key recommendations are:

- The engine must be closely monitored for temperature, oil and gas build up and de-lamination of the mounting plate.
- A sliding calibration factor for the air data boom should be developed to allow for more accurate measurement of in flight data.
- CFD simulation of drag reduction due to a redesign of the fuselage and addition of an engine cowling should be performed.
- Flight testing should focus on verification of results obtained from wind tunnel testing. The data should also be used to update the dynamic model.
- Further development of the dynamic simulation should include addition of the autopilot and navigation sensors.

Page intentionally left blank

TABLE OF CONTENTS

LIST OF FIGURES

LIST OF TABLES

NOMENCLATURE

b	wing span
c	mean wing aerodynamic chord
$\bar{c}$	mean geometric chord
C_L	lift coefficient
C_D	drag coefficient
S	surface area
α	angle of attack
β	sideslip angle
δ_a	aileron deflection
δ_e	elevator deflection
δ_r	rudder deflection
δ_t	thrust setting
$C_{l\beta}$	rolling moment due to sideslip
$C_{l\delta a}$	rolling moment due to aileron deflection
$C_{l\delta r}$	rolling moment due to rudder deflection
C_{lp}	roll damping derivative
C_{lr}	rolling moment due to yaw rate
C_{m0}	pitching moment at zero angle of attack
$C_{m\alpha}$	aircraft pitching moment curve slope
$C_{m\delta e}$	pitching moment due to elevator deflection
C_{mq}	pitch damping derivative
C_{mu}	pitching moment coefficient due to flight velocity
$C_{N\delta a}$	yawing moment due to aileron deflection

$C_{n\beta}$	yawing moment due to sideslip
$C_{n\delta a}$	yawing moment due to aileron deflection
C_{ndr}	yawing moment due to rudder deflection
C_{nr}	yaw moment damping derivative
C_{np}	yaw moment due to roll
C_{X0}	force coefficient in x-direction at zero angle of attack
C_{Xu}	force variance coefficient in x-direction due to flight velocity
C_{Xa}	force variance coefficient in x-direction due to angle of attack
C_{Xde}	force variance coefficient in x-direction due to elevator deflection
C_{Xdt}	force variance coefficient in x-direction due to thrust
C_{Yr}	side force due to yaw rate
$C_{Y\beta}$	side force due to sideslip
$C_{Y\delta a}$	side force due to aileron deflection
$C_{Y\delta r}$	side force due to rudder deflection
C_{Yp}	side force due to roll
C_{Ydt}	variance coefficient in y-direction due to thrust
C_{Z0}	force coefficient in z-direction at zero angle of attack
$C_{Z\alpha}$	force variance coefficient in z-direction due to angle of attack
C_{Zq}	force variance coefficient in z-direction due to pitch rate
C_{Zu}	force variance coefficient in z-direction due to flight velocity
C_{Zde}	force variance coefficient in z-direction due to elevator deflection
C_{Zdt}	variance coefficient in z-direction due to thrust
φ	roll angle
ψ	yaw angle
θ	pitch angle

m_c	mass ratio non-dimensionalized to wing chord
m_b	mass ratio non-dimensionalized to wing span
p	roll rate
q	pitch rate
r	yaw rate
u	velocity in x-direction
v	velocity in y-direction
w	velocity in z-direction
$\hat{u}$	non-dimensional velocity in x-direction
V	free-stream velocity
$\bar{q}$	dynamic pressure
g	gravity
W	weight
6DOF	six-degree-of-freedom
DCM	direction cosine matrix

1. INTRODUCTION

This year the Aerodynamics and Propulsion group was tasked with a number of key project objectives. The engine needed to be started and broken-in. Throttle and choke controls needed to be designed and built for use on the prototype. The fuel system design needed to be modified for the prototype and installed in the fuselage. An air data boom needed to be designed, manufactured and tested for use on the prototype. A drag reduction study needed to be undertaken using Computational Fluid Dynamics (CFD), focussing on redesign of the nose cone. A mount for the wind tunnel model needed to be designed and manufactured and successful wind tunnel tests needed to be performed. An analysis of the aircraft performance during take-off needed to be performed and the dynamic simulation needed to be further developed from a linear model to a non-linear model. This report will explain the work completed on these tasks, as well as provide recommendations for future project teams.

2. PROPULSION OVERVIEW

This year, propulsion worked with the engine and fuel system for the prototype. At the beginning of the year, the engine was mounted on a test rig, almost ready for first start, and there was a conceptual design for the fuel system. Major tasks accomplished were: first start and break-in of the engine, design of the choke and throttle controls for the engine, and design modification and assembly/installation of the fuel system.

3. POWERPLANT

At the beginning of the semester, the engine was almost ready for first start. The two tasks which needed to be completed were construction of a new control panel, and design of a throttle control, and their designs are shown in DR93-04. It was decided to attach the control panel directly to the test rig to allow easier monitoring of the engine during operation, and simplify the controls required. A lawnmower throttle assembly was incorporated into the control panel for operation of the throttle and a bracket was built.

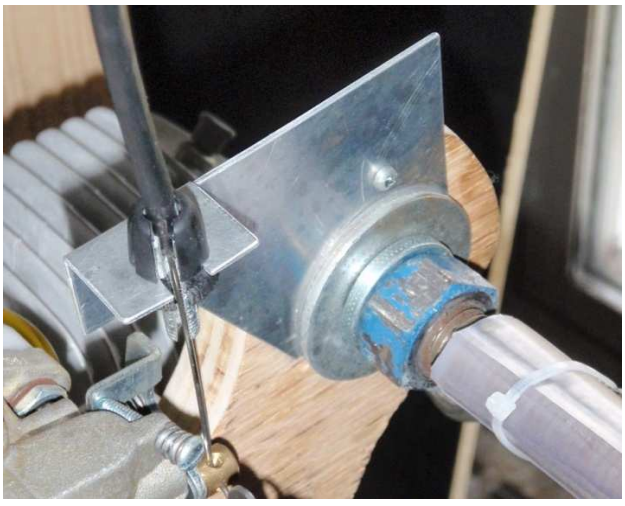

Figure B - 1: Throttle bracket

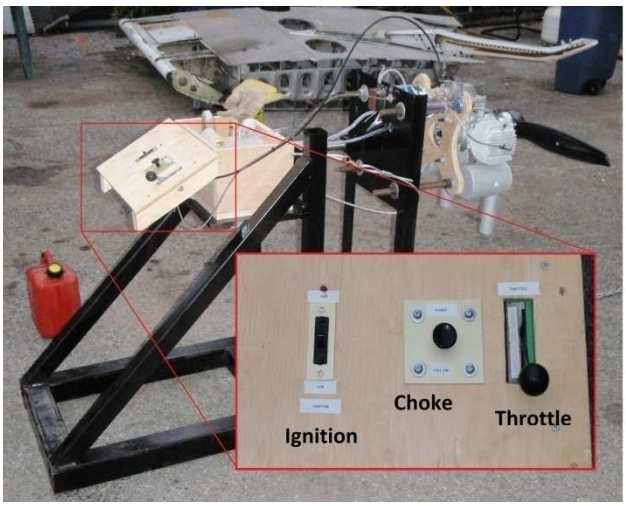

Figure B - 2: Test rig with control panel

3.1 First Start and Break-in

After the preparations were completed, the first start was attempted on 08 October 2008. The engine was started 3 times, but would stop after 1 second. Also on the third attempt, one of the mufflers separated from the engine. The cause of this was determined to be incorrect length of bolt and poor design of muffler attachment. Further engine testing was completed without mufflers.

3.1.1 Operation

Issues persisted with the engine only starting for 1 to 2 seconds. Two experienced model aircraft operators were consulted and assisted with the next test run. The problem was the spark plug caps. Their design requires that they be pushed very forcefully to completely mate with the spark plug. After this, the engine had no issues with running. The engine was also mounted inverted on the test stand to simulate the way it will be mounted on the fuselage.

Initial break-in runs were sustained for approximately 10 minutes – the maximum duration achievable, given the size of the fuel tank. Once the testing group was comfortable with the operation of the engine, runs were extended to 30 minutes. In temperatures below zero, there have been no issues with overheating the engine, but when operated in the summer, the engine temperature should be closely monitored to ensure the engine does not overheat.

3.1.2 Engine Mounting

The Propulsion group only worked with mounting the engine to the mounting plate, attaching the mounting plate to the fuselage was the responsibility of the Fuselage group. Mounting the engine to the mounting plate is outlined in DR103-02. Initially, the engine was mounted to the engine mounting plate (also referred to as the engine box) using the rubber vibration mounts provided by the manufacturer. During operation, the cylinder heads and carburetor showed a displacement of +/- 3cm due to the vibration of the engine. Since the engine is mounted so close to the fuselage, this was unacceptable, so the rubber bushings were replaced with aluminum ones. Consultation with modellers who operated similar engines confirmed that hard mounting the engine is a common practice for engines of this size.

The vibration of the engine also caused the first plywood mounting plate to delaminate. This was replaced by 16 ply beech plywood. This high grade plywood was used for the rest of the break-in/testing with no issues. When operating the engine on a newly manufactured mounting plate, the bolts must be checked often as the plywood will compress. Testing has shown that the plywood will be fully compressed after approximately 30 minutes of engine time.

3.2 Engine Controls

The other large task for the Propulsion group was to design and build the engine controls for the prototype. These include the throttle and choke. Details of the engine control design are in DR103-02. The proximity of the engine to the fuselage (2.75 inches) and the vibration of the engine were both instrumental in driving the current design of the engine controls.

3.2.1 Throttle

The throttle assembly uses the same servo as all of the other control surfaces. A small aluminum bracket was designed to hold the throttle. The servo is connected to the throttle actuator arm, by a semi-flexible plastic pushrod. This will ensure the vibrations are not transmitted directly back to the servo.

3.2.2 Choke

The choke is only required during the starting sequence, therefore, there was no servo required to operate it. Initially, the pushrod is placed in the "ON" position, and the engine is turned over. Once the engine begins to cough, the pushrod is placed in the "OFF" position and the engine can then be started. The choke control will be operated by the individual who is starting the engine.

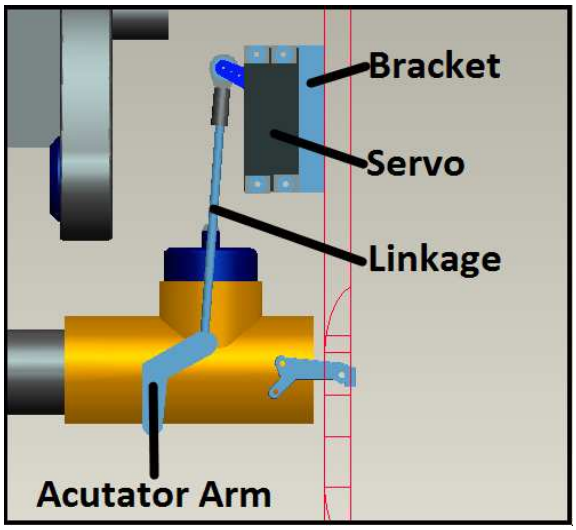

Figure B - 3: Throttle assembly

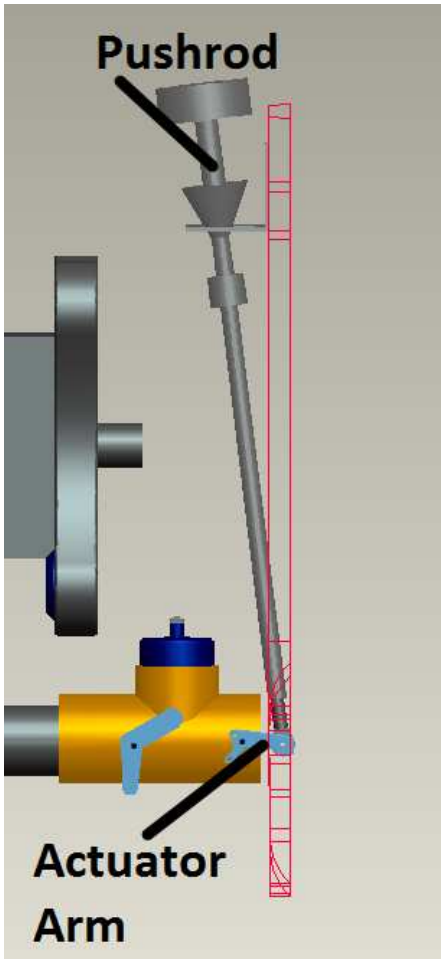

Figure B - 4: Choke assembly side view

3.3 Conclusions

The following section contains the conclusions for the work that was completed by the propulsion sub-group:

- Break-in and testing has confirmed that the engine will be suitable, and provide enough power for the UAV.

- Vibrations have been a huge issue this year. All components must be designed to withstand them.

3.4 Recommendations

- Closely monitor engine temperature during ground operations, a leafblower could be used to provide extra cooling.

- Low idle setting on the carburetor will have to be set with mufflers mounted on the engine, as all testing was done without mufflers.

- Because the mufflers will also be mounted "inverted", they should be checked to ensure there is no build up of oil or gas that could not drain

- The engine mounting plate should be monitored for de-lamination

- The MS21044N6 self locking nuts used on the engine mounting **MUST NOT** be re-used. Once the bolts have been removed, they **MUST** be replaced with fresh nuts as the used ones will not retain their self-locking capacity.

4. FUEL SYSTEM

A complete design for the fuel system was received from the 2007/2008 team. Upon review, it was determined to modify the design, as it pertained more to the final product rather than the prototype. The changes and reasons for each are outlined in DR93-05. The changes are summarized in the table below. The lead engineers were consulted while making these decisions. The elimination and/or modifications save weight and money.

Table B - 1: Modifications

Modification	Reason
Solenoid fuel shutoff removed	Fuel pump design cuts fuel flow when ignition shut off
Fuel flow meter removed	Deemed unnecessary for short duration of test flights
Fuel tank changed	Will use a model similar to the tank on the test rig.
Fuel level sensor removed	Deemed unnecessary for short duration of test flights

The modifications of the fuel system were also done to ensure the fuel system would conform to the necessary standards so the UAV can receive its operating certificate.

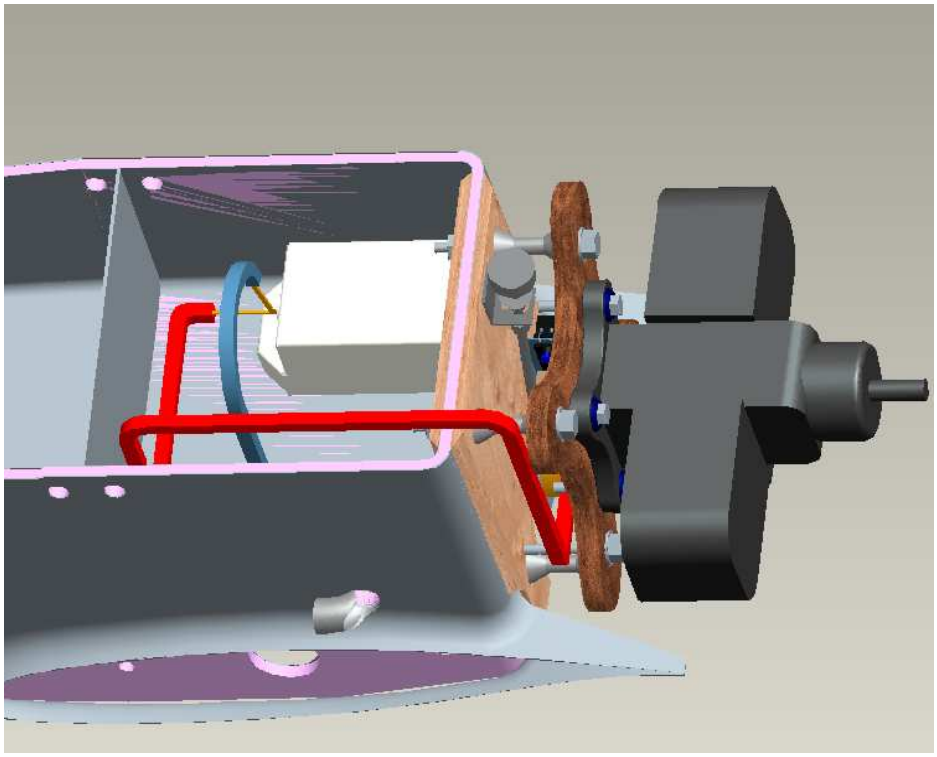

Figure B - 5: Fuel system

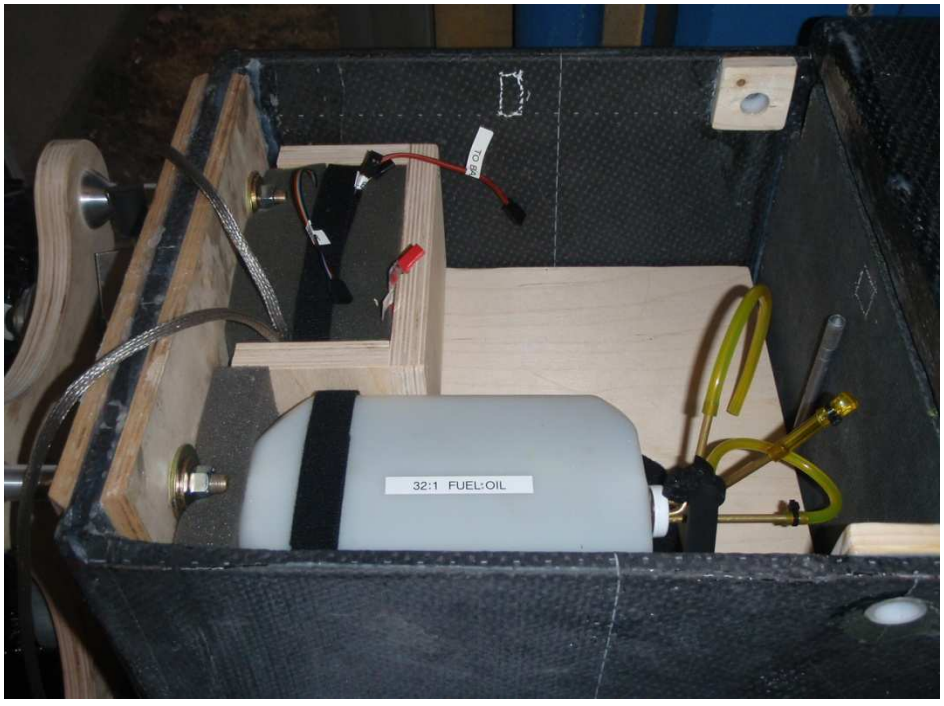

Figure B - 6: Inside the fuel bay

A wooden assembly was also designed to fit in the fuel bay of the prototype to serve as a place to mount the fuel tank, battery, and ignition module. A box from AVI will also be installed on the assembly. All wood used on the prototype must be sealed with epoxy resin to ensure it will not absorb moisture or fuel. Detail drawings of all fuel system components and assemblies can be found in DR93-05.

5. AIR DATA BOOM OVERVIEW

The need for an air data boom was recognized last year for completion of flight testing and post flight analysis of UAV flight performance. After communication with various boom manufacturing companies, it was made evident that an air data boom would not fit into the project budget; thus, one would have to be designed and manufactured as part of the project work this year.

Throughout the academic year, various boom configurations were presented to the project group, until a final configuration was selected. Theoretical static pressure distributions were found from research and used to determine the optimal locations of each of the boom components, so as to minimize the overall blocking force imposed on the static pressure taps.

A full drawing assembly package was produced for the air data boom, which was followed carefully during the manufacturing process. All dimensioned tolerances were met, and only minor changes were made to the air data boom geometry. Wind tunnel testing was then performed in order to assess both the raw boom performance (through analog measurement), and the overall performance of the data acquisition system. Further testing using turbulence grids was performed in order to introduce a worst-case flight scenario.

5.1 Measurement requirements

GeoSurv II has several performance requirements that must be met, as outlined in both the SRD and airworthiness standards, and summarized in DR 93-02. In order to meet the performance requirements, a flight test plan has been developed. This flight test plan calls for a nose boom installation that is capable of measuring the following flight data: angle of attack (AOA), angle of sideslip (AOS), total pressure, and static pressure.

5.2 Methods of measurement

There exist several methods for measuring AOA, AOS, total pressure and static pressure. As such, various methods were investigated, and various conceptual boom configurations were developed. This process is described fully in DR 93-02.

5.2.1 AOA and AOS

The first boom configuration included a multi-hole probe, in which AOA and AOS could be measured as a pressure gradient about a central tube that is always exposed to the total pressure. This gradient is measured horizontally (AOS) and vertically (AOA) by finding the difference in pressure between tubes located at 45 degrees on either side of the central hole. Although the multi-hole probe provided an all-in-one solution for measuring the required data, research and discussions with Carleton graduate students determined the following: calibration of such a

precise instrument is extremely tedious and requires a high degree of accuracy, multi-hole probes are sensitive to high angles of attack, and re-calibration is required after significant vibration, jarring, or particle build-up, which could essentially make all in-flight readings meaningless.

It was determined that directional vane assemblies could provide a more direct measurement of AOA and AOS. It had been discussed that wireless cameras were to be mounted on the UAV for recording the flights; and thus, it was suggested that these cameras also be used to monitor vane deflection. Another full, conceptual boom design was produced which incorporated the wireless cameras, but it was determined that synchronization of the video feed with the rest of the flight data (to be recorded by the onboard micropilot system) would not be feasible. This meant that post-flight data analysis could not consider all flight data simultaneously for performance assessment.

Further research was conducted into encoders, angular transducers, and potentiometers for direct angular measurement of the vane assemblies. Potentiometers were selected as they are relatively inexpensive and can provide a precise analog voltage, which is required by the micropilot system.

A conceptual vane assembly was then developed which incorporated the potentiometers as angular measurement devices. The conceptual vane assembly design is shown below in Figure B - 7:

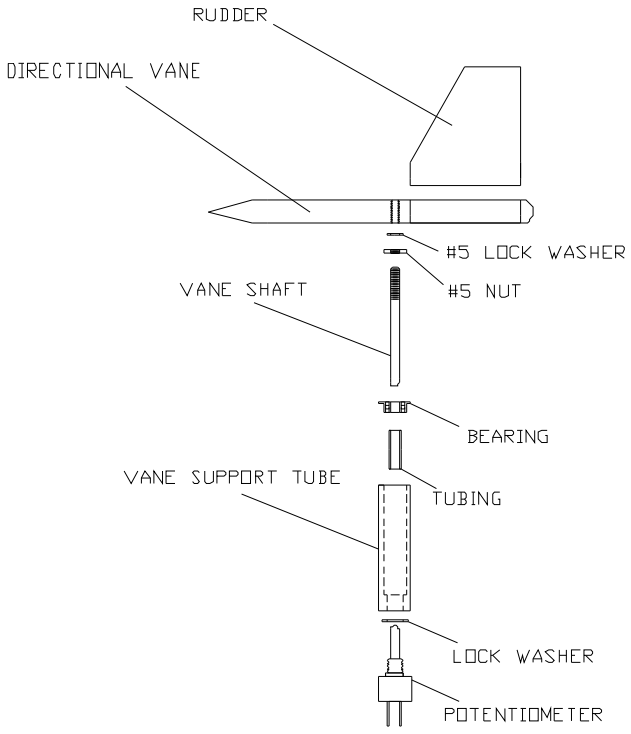

Figure B - 7: Conceptual vane assembly

5.2.2 Total and Static Pressure

Pitot-static installations are commonly used for measurement of total and static pressure. These installations operate on fundamental principles of fluid dynamics, in which the total pressure is measured at the tip of the probe, and static pressure is measured using static taps which are located along the side of Pitot probe (transverse to the flow). One major limitation of Pitot-static systems is the effect of probe inclination to the free stream, which introduces error in pressure readings. It was determined that a Pitot-static installation would be used on the air data boom, but slight modifications were considered for improvement of performance.

The multi-hole probe, as discussed in the previous section, offered a solution for total pressure measurement, and static taps could easily be drilled along the side of such a probe. However, due to reasons discussed, this option was not selected.

From research, the idea of a Kiel shield was spawned, which is essentially a bell-mouth inlet that is placed over the Pitot probe. This inlet can significantly extend the range of inclination of the Pitot probe relative to the free stream, as discussed in DR 93-02. A conceptual Kiel shield design was developed, in which all dimensions were specified as functions of the inlet diameter size, allowing the design to be scalable to an appropriate size for the boom. This design can be seen below in Figure B - 8:

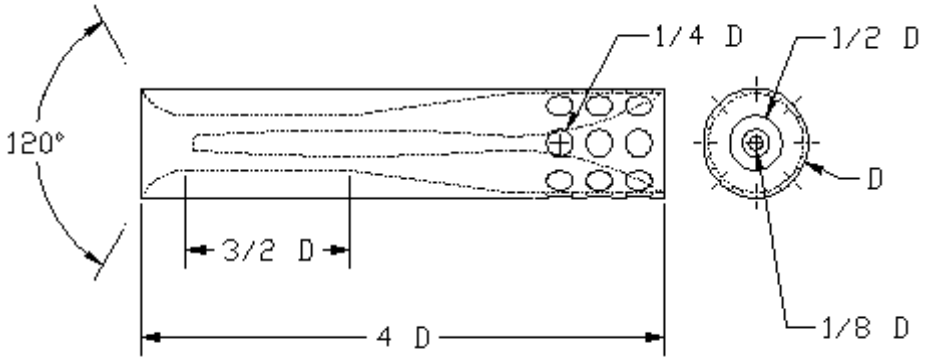

Figure B - 8: Conceptual Kiel shield design

It was determined that incorporating such a shield would improve boom performance; thus, the Kiel shield and Pitot-static probe were selected as air data boom components.

5.3 Air Data Boom design

After the appropriate methods were selected for air data measurement, a full boom layout was developed. A summary of the boom design process is included in DR 93-09C. This report also includes the full assembly drawing package that was developed for boom manufacturing.

The air data boom was manufactured in the Carleton machine shop, as discussed in DR 103-05, and attention was paid to adhere to the specified tolerances. Figure B - 9 shows an overview of the boom layout and provides a visual comparison between the boom design and the manufactured boom:

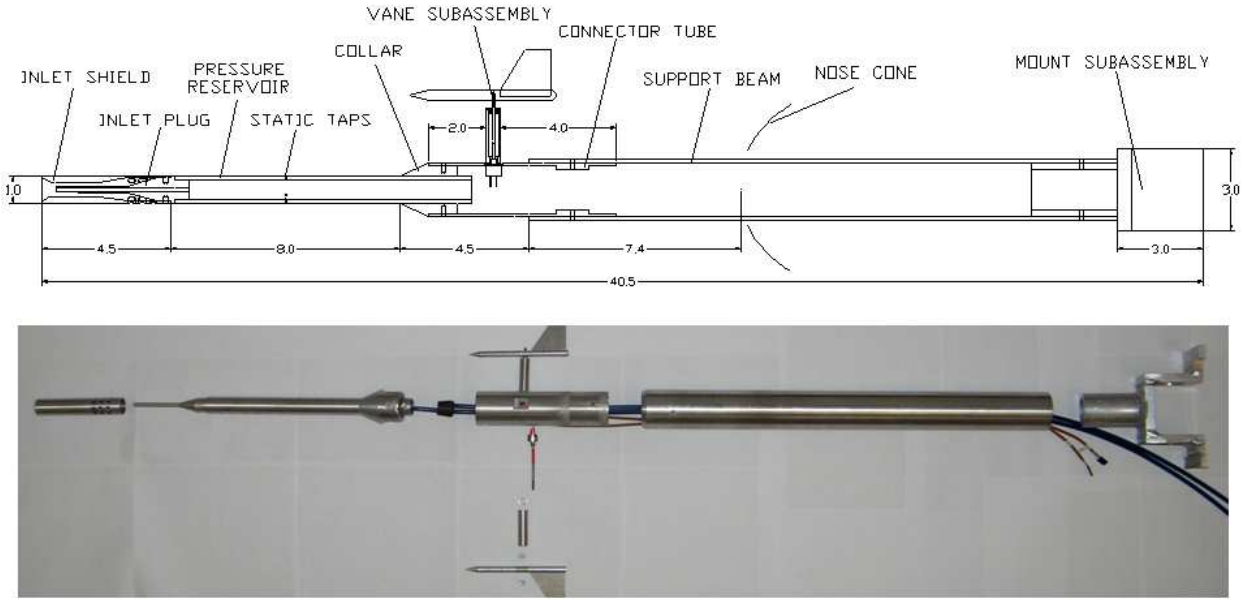

Figure B - 9: Boom layout overview

Electrical leads and pressure tubing run throughout the interior of the boom, which connect the sensing elements to circuitry in the avionics bay. These interconnections are labelled in Figure B - 10 below:

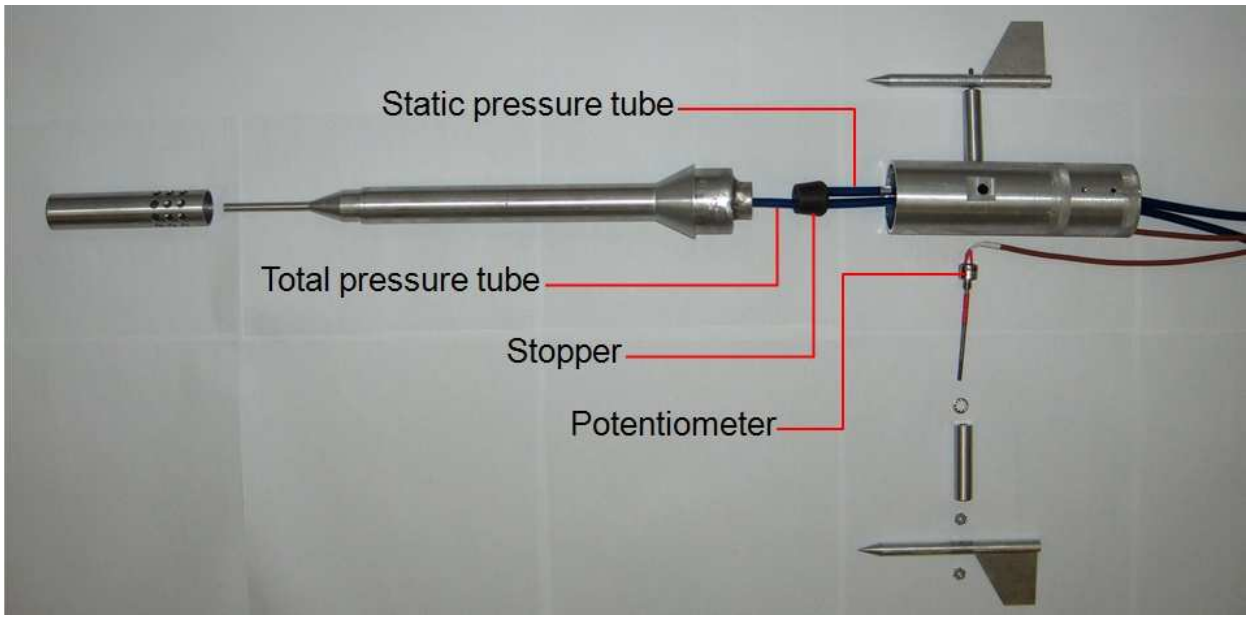

Figure B - 10: Boom sensor interconnections

The stopper shown in the above figure is used to seal the static pressure reservoir. Two holes pass through the stopper: one for the total pressure tube (which is bonded to the back of the inlet plug), and one for the static pressure tube.

A breakdown of the air data boom weight by component is given in the table below:

Table B - 2: Boom component weights

Segment	Volume (m^3)	Mass (kg)
Inlet shield	1.9305E-05	0.0692
Inlet plug	1.8098E-06	0.0424
Pressure reservoir	5.8419E-05	0.1577
Collar	2.6813E-05	0.0723
Vane subassembly	8.0961E-06	0.1302
Connector tube	4.2230E-05	0.2964
Support beam	2.8033E-04	0.7568
Mount assembly	2.9496E-04	0.9788
Tubing/wiring	-	0.045
	Total	**2.5494**

5.4 In-Flight Reaction Forces

An analysis was required of the in-flight reaction forces to be experienced by the nose cone and the boom mount. In order to perform this analysis, the following simplifying assumptions were made:

- The boom was considered to be 37.5 inches long with a weight of 15.40 N (the mount assembly was not considered part of the boom)
- The boom geometry was assumed to be cylindrical with a constant diameter of 2 inches
- The nose cone was assumed to be a simple
- Pin support with a reaction force that always acted in the opposite direction of loading (in the y-direction only)
- The centre of gravity was assumed to be at the middle of the boom (18.75 inches along the boom length)

The following three boom loading conditions were considered in the analysis: static loading, landing, and aerodynamic loading, as shown in Figure B - 11 below:

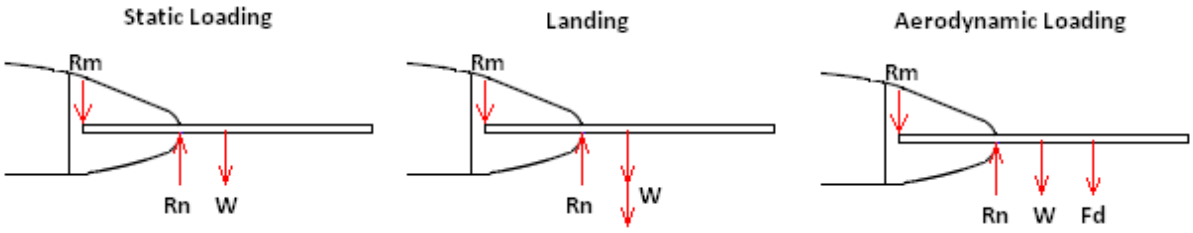

Figure B - 11: Boom loading conditions

As discussed in DR 93-09C, the following reaction forces were found for each of the loading conditions.

- At static loading, R_N=22.22 N [up], and R_M=6.81 N [down]
- During landing, R_N=56.06 N [up], and R_M=17.19N [down]
- During maximum aerodynamic loading (at dive velocity and 19-degree inclination), R_N=41.26 N [up], and 16.05 N [down] for R_M

It was determined that maximum loading would be experienced on landing, and the recommendation was made to the structures team nose cone reinforcement layers be added that could withstand up to 80 N of loading, to allow for a safety factor in the design.

5.5 Testing and Calibration

In order to assess the measurement accuracy of the air data boom, a wind tunnel mount (beam) was built that could interface with the existing struts, balance, and wind tunnel section used for previous UAV project testing.

The experimental test setup can be seen in Figure B - 12 below:

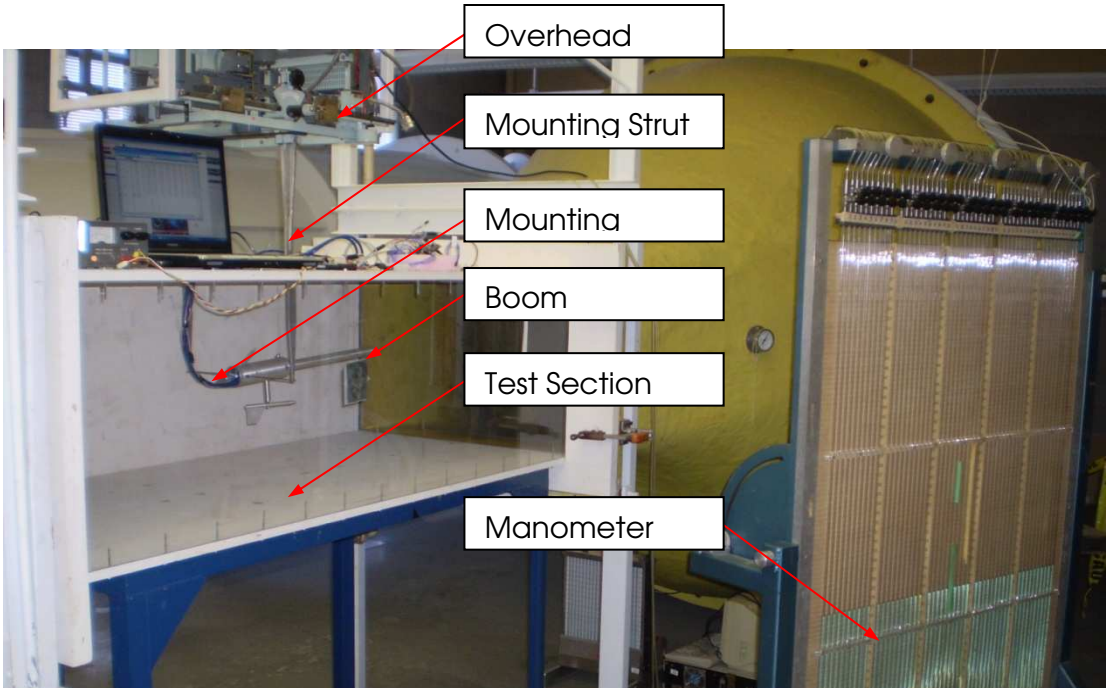

Figure B - 12: Wind tunnel test setup

Calibration of the sensing elements (potentiometers, pressure transducers) was performed according to the procedure outlined in DR 104-03. This ensured that the pressure transducers indicated atmospheric pressure, and that the potentiometers indicated zero degrees when the vanes were in line with the air data boom.

5.5.1 Raw Performance

Initial testing of the air data boom involved static positioning of the boom at incremental angles of attack and angles of sideslip. For each position, the wind tunnel speed was increased (incrementally) from the theoretical UAV stall speed of 36 knots to 85 knots, as limited by the wind tunnel.

The multi-tube manometer shown in Figure B - 12 was used to take readings of the static and total wind tunnel pressures, as well as the static and total pressures sensed by the air data boom. All manometer readings were taken relative to atmospheric pressure.

The velocity readings from the boom (Vb) were compared to the velocity readings from wind tunnel (Vw) for various angles of attack and sideslip. The following plots were created:

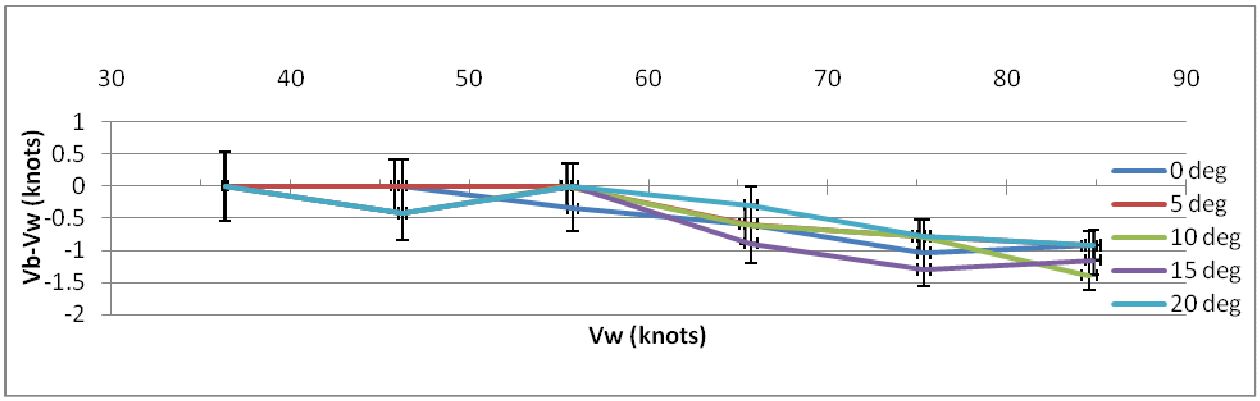

Figure B - 13: Boom velocity reading versus reference speed for an AOA sweep

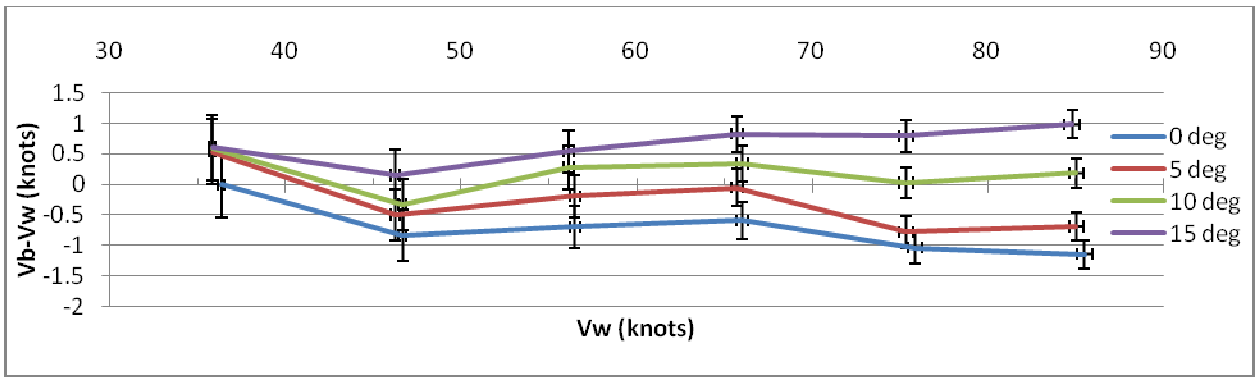

Figure B - 14: Boom velocity reading versus reference speed for an AOS sweep

In Figure B - 13, it can be seen that the velocity reading indicated by the boom (as read by the multi-tube manometer) is consistently below the wind tunnel reference speed. This difference increases as the velocity increases, up to a maximum difference of -1.39 knots (for 10 degrees AOA at 85 knots).

In Figure B - 14, it can be seen that the velocity readings indicated by the boom (as read by the multi-tube manometer) increase (with respect to the wind tunnel reference speed) as the AOS is increased. As shown by the trend, an incremental increase in AOS of 5 degrees results in a vertical shift in the indicated boom velocity by 0.5 knots. This corresponds to an increase of 0.1 knots per degree of AOS.

5.5.2 Air Data Acquisition System Performance

Dynamic testing of air data boom performance was conducted using the data acquisition system. An overview of the data acquisition system is shown in the block diagram in Figure B - 15 below:

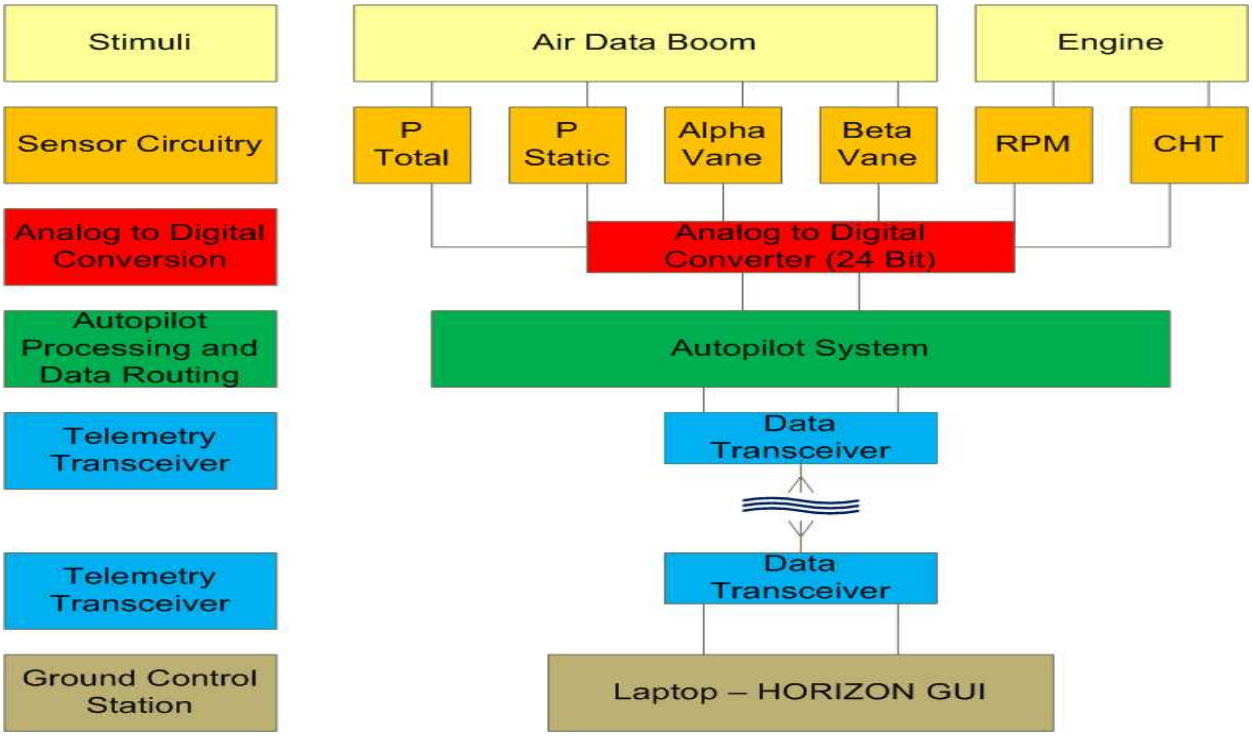

Figure B - 15: Data acquisition system overview

The engine sensors were not involved in wind tunnel testing, and the (wireless) data transceivers were only used briefly while observing the logging capabilities of the ground control station; therefore, the autopilot system was directly connected to the ground control station (laptop) for the majority of dynamic testing. A description of the data acquisition system and its components can be found in DR 94-03.

Dynamic test runs were performed by setting the wind tunnel to a constant speed (in the range of 36 - 85 knots), and actuating the boom (manually, at a constant rate) between +20 and -20 degrees. It was observed that the vanes remained aligned with the free stream at all times during testing.

Sample plots of AOA versus time and speed versus time were constructed from the logged data of a dynamic test run at 55.4 knots and included in Figure B - 16 and Figure B - 17 below:

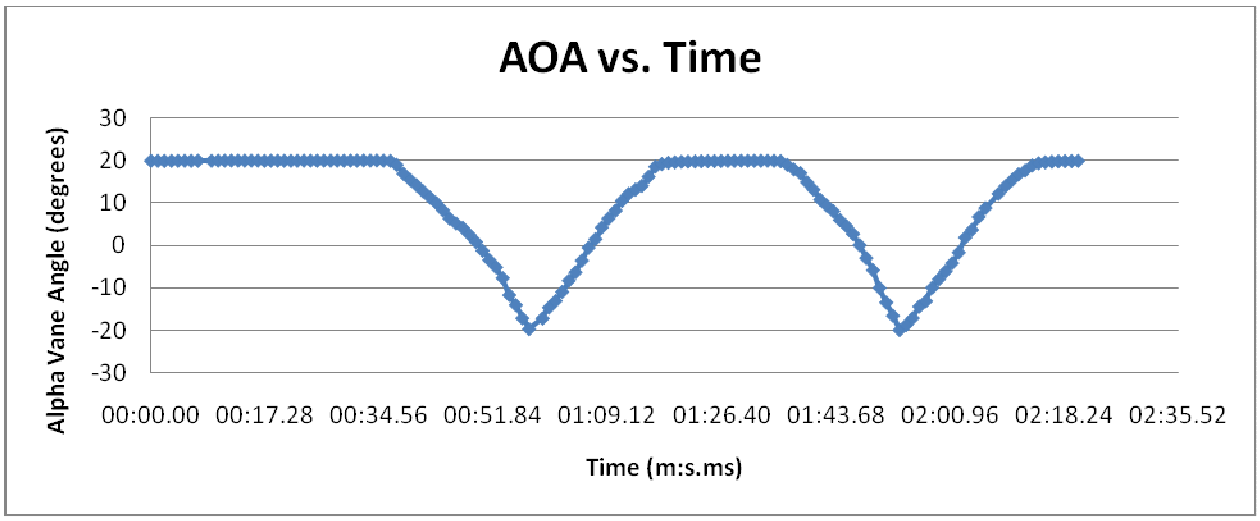

Figure B - 16: Boom AOA reading during dynamic AOA sweep

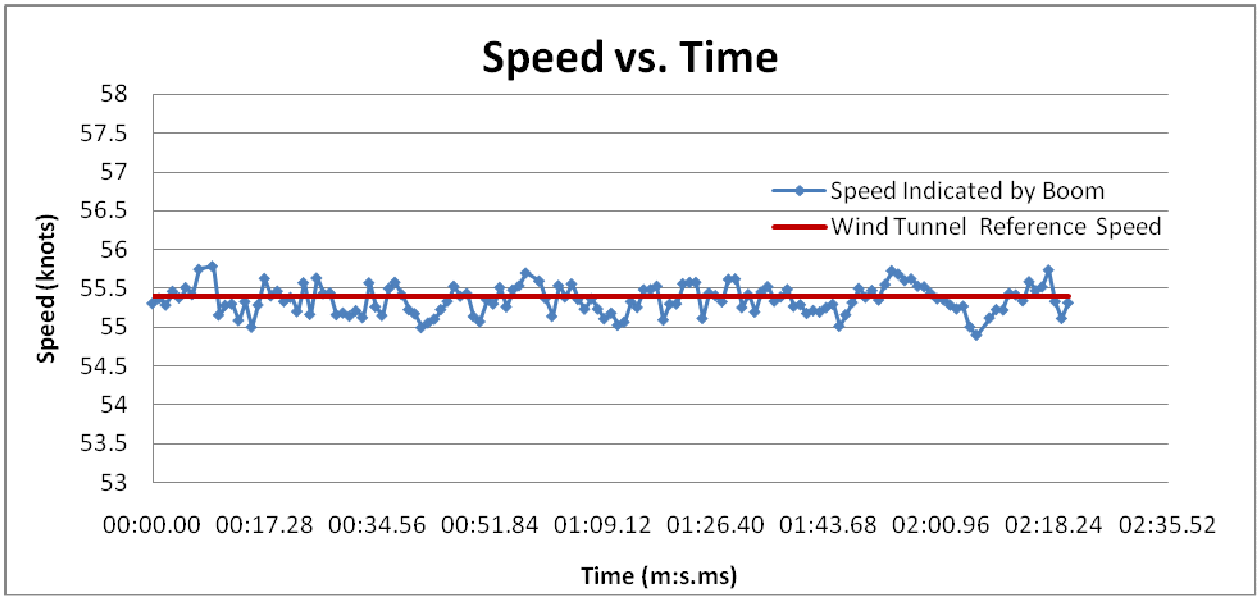

Figure B - 17: Boom velocity reading during dynamic AOA sweep

At 55.4 knots, it was observed that throughout the 140 second test run, the speed indicated from the boom pressure transducer readings were always within 0.5 knots of the wind tunnel reference speed. At 74.9 knots, it was found that throughout a 140 second test run, the speed indicated from the boom pressure transducer readings were always within 0.6 knots of the wind tunnel reference speed.

Dynamic testing was found to eliminate monometer reading errors (from raw performance testing), and yield velocity readings from the air data boom that were within 0.6 knots of the wind tunnel reference speed. This is discussed further in DR 103-06.

Turbulence testing was also performed, in which a turbulence screen with 12% intensity was used (corresponding to a worst-case scenario, in which the UAV would not be able to maintain

flight). Boom velocity readings were found to be within 2 knots of the wind tunnel reference speed of 55.4 knots.

5.6 Conclusions and Recommendations

An air data boom was designed and manufactured this year as part of a data acquisition system that will facilitate UAV flight testing by accurately measuring the required data, providing in-flight data readings, and logging data for post-flight analysis. The following conclusions were made from this year's work regarding the air data boom:

- Vane assemblies were incorporated to measure AOA and AOS
- Total and static pressure will be measured by a Kiel probe and static taps, respectively
- A complete assembly drawing package was produced and used to manufacture the boom. It can be used if future manufacturing is required (ie: if the boom is damaged)
- In-flight reaction forces were analyzed and the recommendation was made that the nose cone be reinforced to withstand up to 80N of loading
- Wind tunnel testing and calibration was performed, during which:
    - Static testing suggested indicated boom velocities accurate to within +/- 1.2 knots
    - Dynamic testing (with the complete data acquisition system) suggested velocity readings accurate to within +/- 0.6 knots
- Turbulence testing was performed using 12% intensity (at 55.4 knots), during which velocity readings were accurate to within +/- 2 knots

The following recommendations were made for continued development of the data acquisition system:

- All testing should be performed using batteries to power the system, as power supplies introduce electrical noise and additional error in data readings
- A sliding calibration factor should be developed to correct for the indicated velocity reading, as raw boom performance suggests elevated velocity readings due to yaw
- A plug should be manufactured to cover the hole in the nose cone when the boom is not installed

6. DRAG REDUCTION USING COMPUTATIONAL FLUID DYNAMICS

Throughout the academic year a number of nosecone designs were simulated using ANSYS Workbench software to see if the aerodynamic drag force can be reduced. This section describes the different designs considered and the results obtained from the simulations.

6.1 Objective of CFD

The objective of computational fluid dynamics (CFD) for this year was to change the current geometry in order to reduce the aerodynamic drag of the aircraft. In order to achieve this CFD analysis was done on three different components; nose landing gear strut, nosecone and fuselage. Initially the nose landing gear strut was redesign and was simulated to determine the drag reduction compared to that of the previous year. Several designs of the nosecone were simulated in CFD in order to compare the values with that of the current design. Modifications to the current fuselage geometry were also considered to investigate the drag benefits from just rounding the fuselage corners.

6.2 CFD of New Landing Gear Design

As recommended from last year's CFD analysis the nose landing gear was redesigned in order to reduced the aerodynamic drag. This was primarily because the CFD analysis using the old landing gear design showed a drag increase of 35% when compared to the drag created with no landing gear. A design was proposed by the structures group that instead of having a flat plate landing gear it would be a cylindrical shaped nose landing gear. By using this shape the total drag was reduced by 7%. The reason behind this drag decrease is in the flow separation that occurs aft of the nose landing gear, the cylindrical shape nose landing gear delays the separation which decreases the pressure drag, and because the landing gear is considerably long it has a large impact on the drag values, DR93-01 shows the simulation results in more details.

Due to redesign of the main landing gear whereby it uses two cylindrical shaped struts, it is expected that the drag values will change again. The old design of the main strut composed of a flat plate that is aligned with the flow, which has a lower drag coefficient than a cylindrical shape and will further increase the drag coefficient of the aircraft. In order to further lower the drag values, a fairing at the trailing portion of the cylinder should be considered to avoid separation and further decrease the pressure drag.

6.3 Nosecone Design

6.3.1 Initial Designs

The different nosecone designs that were initially considered were composed of a cylindrical fuselage with a conical and elliptical nosecone as shown by A and B in Figure B-11. With these two fuselage geometries, the drag when compared to that of the current fuselage was reduced by approximately 20 %, as outlined in DR91-03. Although there is a benefit in using a cylindrical fuselage shape, it means that the entire structure has to be reanalyzed. In order to avoid this, the nosecone was redesigned to have smooth and gradual contours that merge tangentially to all surfaces of the fuselage geometry.

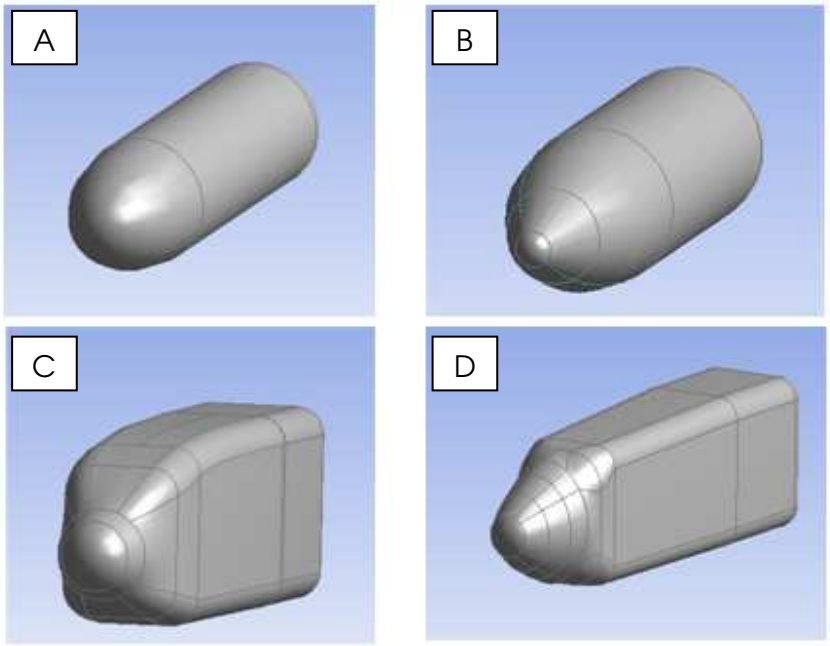

Figure B - 18: Initial designs created using the design modeler in ANSYS

When this concept was implemented into the design of the nosecone there were some problems primarily with generating the desired shape using the design modeller in ANSYS Workbench. Going from a circular to a rectangular cross section was difficult to model, and the simulations also showed that there was no improvement in the drag coefficients as outlined in DR93-07.

6.3.2 Final Nosecone design

The final design that was considered was modeled using Pro/E. This design consists of two elliptical arcs; one that is tangential to the upper surface and one that is tangential to the bottom surface.

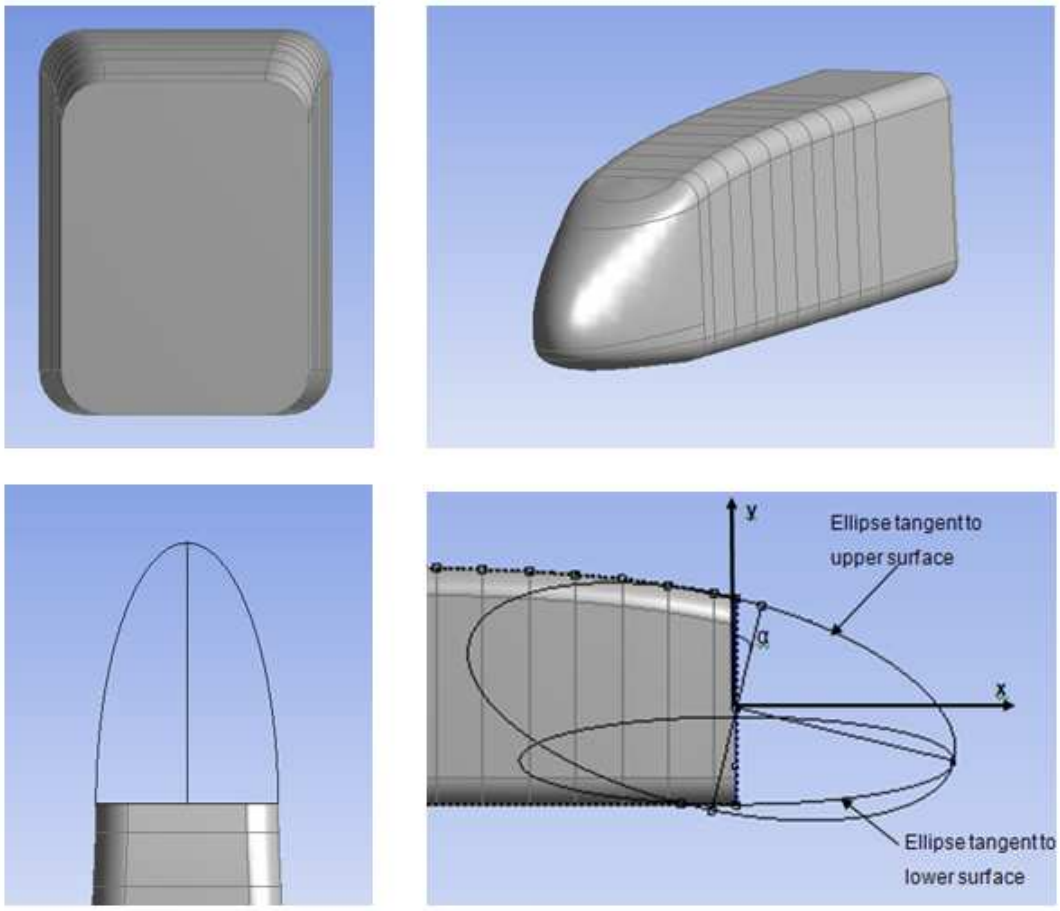

Figure B - 19: Front, side and top view of the new nosecone design

6.4 Simulations Performed

Simulations were performed using the current nosecone and the new design with the current fuselage and a modified fuselage. The different geometries that were modeled is shown in Figure B-13. Simulations were done in order to simulate yawing and pitching flight conditions at different angles of attack and different yawing angles.

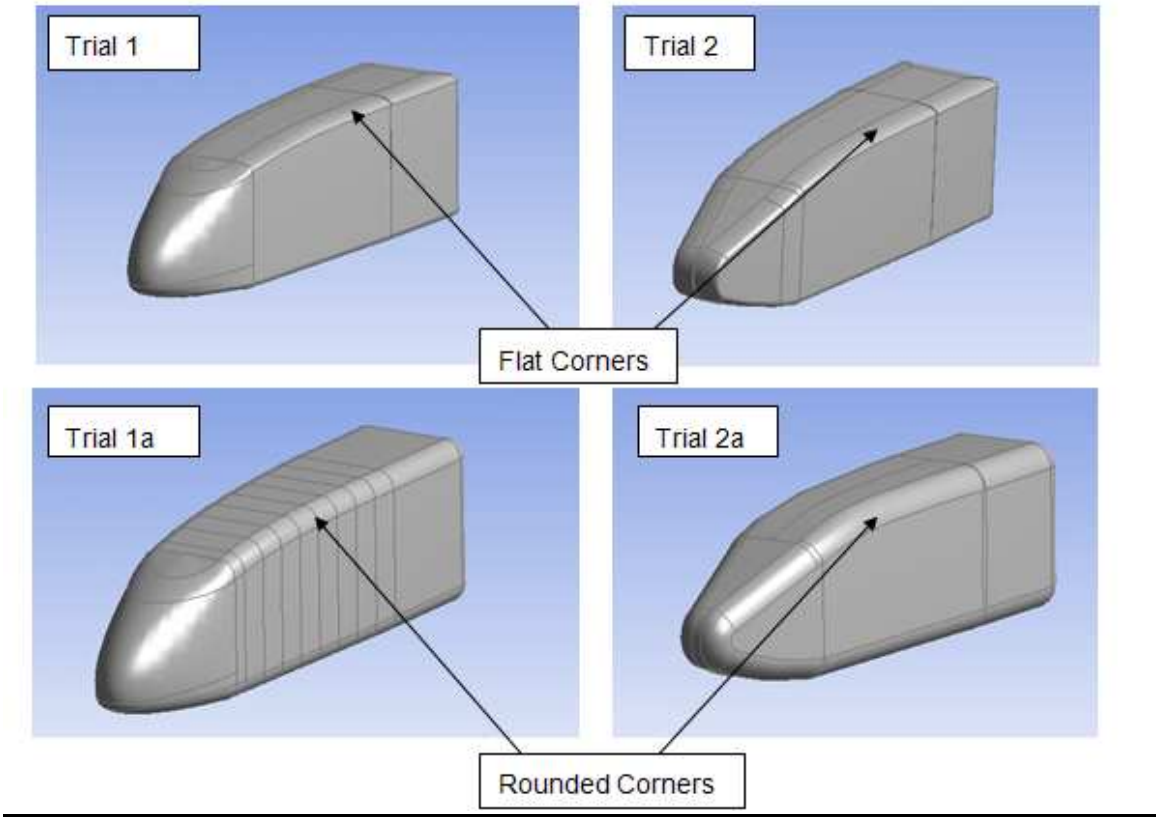

Figure B - 20: Geometry of the fuselage and nosecone simulated in CFX

6.4.1 Mesh Refinement Study

To be certain the simulations were accurate a mesh refinement study was performed, this analysis was done using biased localized mesh. What this means is that rather than refining all the mesh of the domain, only the mesh surrounding the fuselage was refined using point controls option within the CFX mesh. This is an advantage because it allows for controlling the node spacing for each specific sphere thereby concentrating the nodes where the flow gradient is greater. Using this refinement process it was determined that a grid size of 400000 nodes was an accurate yet efficient size in term of computational time. Figure B-14 shows that the drag coefficient stopped changing at about 600000 nodes. It was also found that the difference in the drag coefficient by using 400000 and 600000 nodes was less than 1% difference which indicates an efficient mesh size.

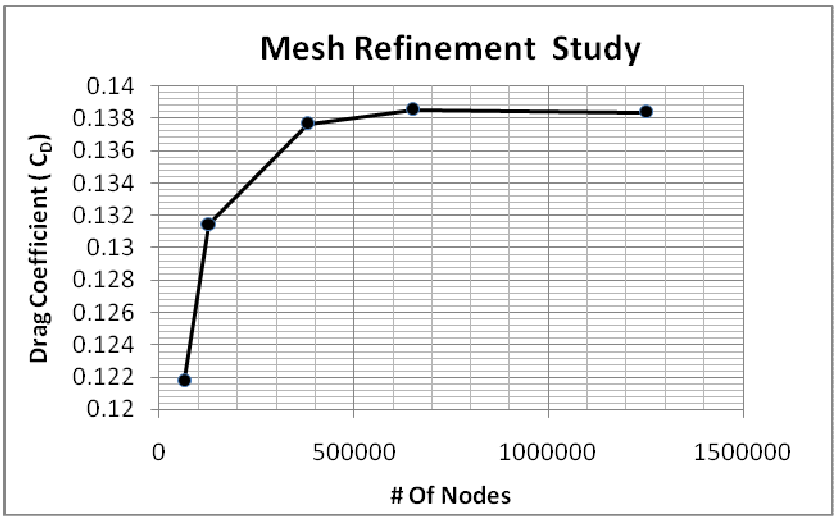

Figure B - 21: Mesh refinement study

6.4.2 Results

The results indicated that the new nosecone designed does very little to reduce drag at low angles of attack , as the angle of attack increases the new nosecone designed actually increases the drag by a very small amount compared to the current design. The simulations showed that with the current nosecone design even at an angle of attack of 15 degrees the flow stays attached. The primary reason for this is that ANSYS CFX assumes a turbulent boundary layer at the inlet and because of this the flow stays attached longer and becomes harder to separate. This makes drag force due to the pressure drag and therefore this should be the best way to reduce drag. By using an unsymmetrical elliptical nosecone shape the net pressure created from the pressure distribution around the nose cone is actually higher than that created by the current nose cone. The lower pressure created by the current nosecone makes for a lower pressure drag, for more details see DR103-09. Figure B-15 indicates that the major contributing factor to the reduction of drag is modifying the current fuselage, by just rounding the corners of the fuselage geometry the simulations indicated a drag reduction of about 10 %, as seen by an entire shift of the curves in the figure.

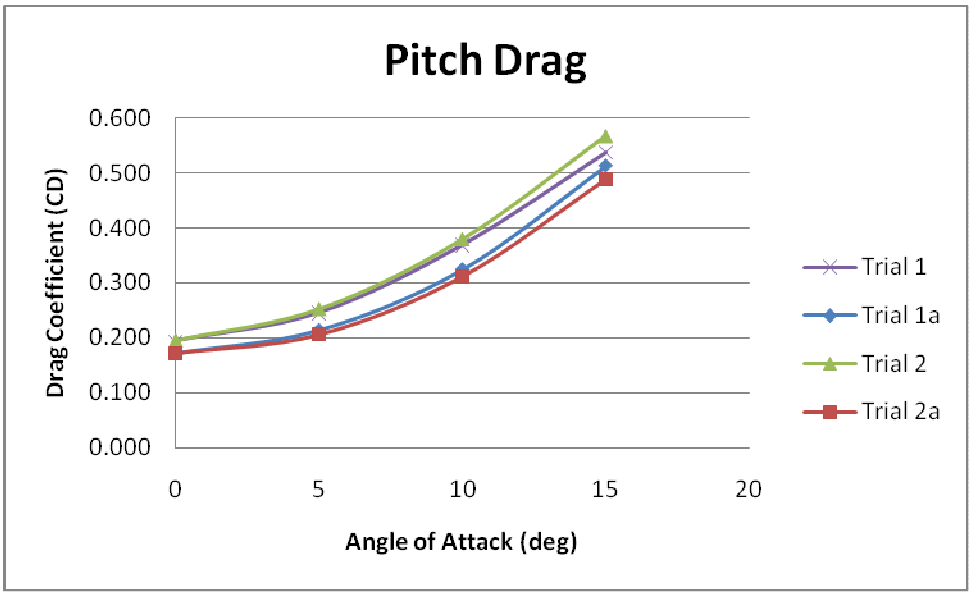

Figure B - 22: Simulation results of the different geometries at different angles of attack

6.4.3 Yawing Results

The yawing results show that the drag is reduced by using the new nosecone design; this was expected because with the new nosecone design separation is avoided. Figure B-16 indicates that by using the new nosecone on the current geometry the drag is reduced considerably, but by just rounding the edges of the current fuselage this drag also is very similar. This shows the benefits of using the new nosecone design, especially for yawing conditions. DR103-09 further discusses these results in detail.

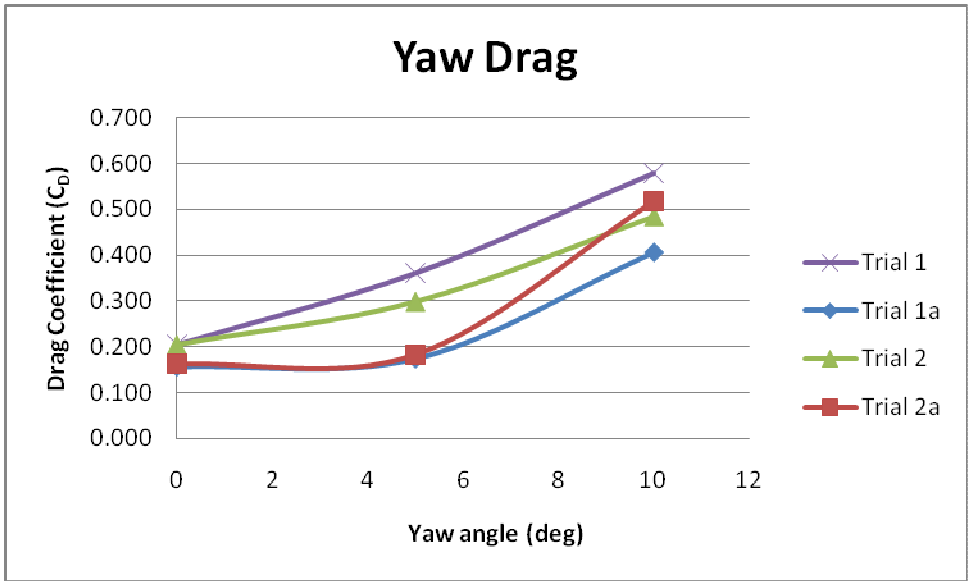

Figure B - 23: Simulation results of the different geometries at different yawing angles

6.5 Recommendations

- To further reduce the drag an engine cowling should be considered, using an engine cowling a large drag can be reduced.

- To further improve this nose cone design other design parameters should be considered; bluntness ration and the fineness ration.

- When assessing this parameters 2D potential flow should be used as it has been indicated the main drag component is pressure drag and the simulations did not indicate any flow separation in the pitch direction at angles below 15 degrees

- Further modification of the fuselage geometry should be considered as the simulations indicate that more drag can be reduced by just rounding the corners of the fuselage.

7. WIND TUNNEL MODEL

The wind tunnel model was inherited from the 2007-2008 project team in a fully built configuration with only minor details requiring attention. The only major component still missing was the support system which would connect the model with the NRC wind tunnel balance.

7.1 Support System Design

At the end of the 2007-2008 academic year, a revised support system design was proposed for supporting the wind tunnel model; however, this design did not meet multiple critical criteria:

- The National Research Council guidelines with regards to the absence of friction locks.

- The requirement for a vertical rather than angled mounting shaft.

- The requirement for a clearly defined fairing around the main shaft in order to minimize the overall drag produced by the model support system.

It was therefore necessary to re-design the entire model support system assembly, as well as, to perform a thorough stress analysis to ensure that it can withstand all loads imposed during the testing period.

The new design for the support system is shown in Figure B-24 and Figure B-25. This design features a pitch selector which can position the model at inclinations of 0^{o}, $\pm 5^{o}$, $\pm 10^{o}$, $\pm 15^{o}$, $\pm 17.5^{o}$, $\pm 20^{o}$ from the horizontal in both upright and inverted attitudes. A set of four pins is used to hold the model in place at each inclination and a centre pin is used to hold the entire assembly together. The model is secured onto the support system using a mounting plate and four bolt screws.

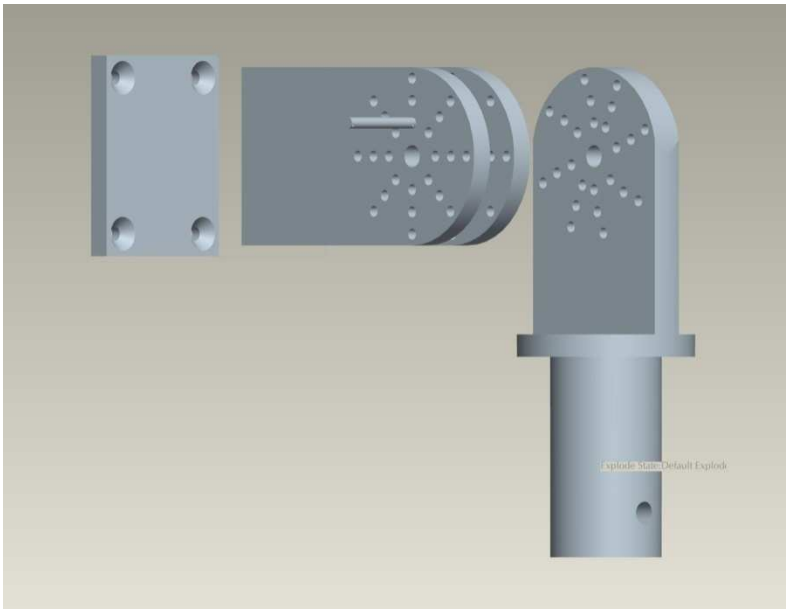

Figure B - 24: Support System Pitch Angle Selector

The support system was initially designed to have a fairing covering the support beam; however, upon consultation with NRC Engineers it was deemed that an interface to one of their fairings would be a simpler approach, thus the design obtained its final shape. Interfacing to the NRC fairing also allowed for the precise positioning of the model at the centre of the wind tunnel thereby simplifying the data collection process.

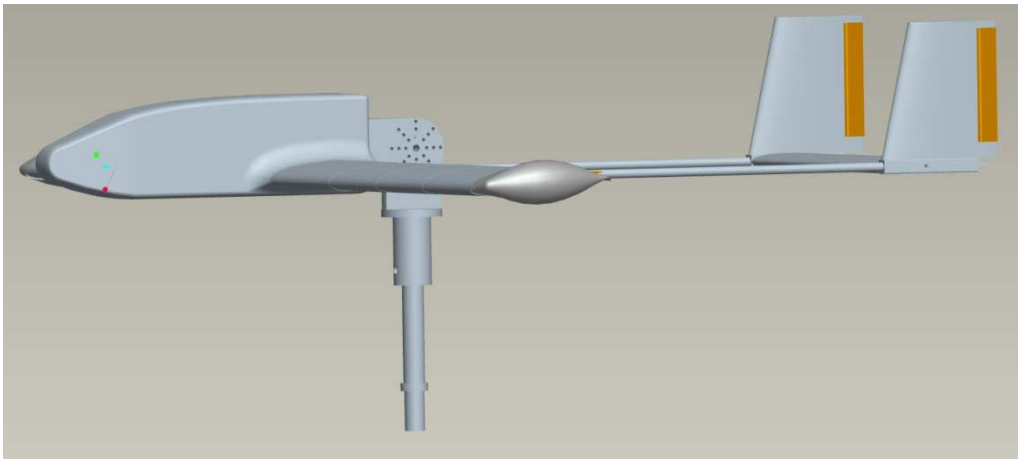

Figure B - 25: Final Scaled Model for Wind Tunnel Testing

With the design complete, a load analysis was performed at the most severe conditions expected during the test runs to determine if the desired safety factor of three could be achieved. The steel plate, bar stock, and high strength pins used to manufacture the support system were found to exceed the safety factor requirement in all cases as shown in DR93-06. Manufacturing of the support system was outsourced to the Carleton University Science Technology Centre in order to meet the tight deadlines imposed by the testing schedule.

7.2 Final Model Preparations

Apart from the manufacturing of the model support system there were a few items left to complete before the model could be taken to the NRC. The pins required for all control surface deflections were cut, bent, and grooved for a correct fit within the model. The overall surface finish of the model was improved by removing a few plastic stubs from the top of the fuselage and by sanding the rusty tail booms to a shine. Once all work had been completed, the model was transported to the NRC in advance of the first test run.

8. WIND TUNNEL TESTING

The plan for wind tunnel testing consisted of two days at the NRC wind tunnel on Montreal Rd one in early November and the other in January in order to gather all necessary data. This would allow enough time to properly process the results and perform follow-up analyses where necessary. The objectives of the tests are to validate analytical and CFD stability predictions, to verify new methods for meeting the descent gradient requirement, and to obtain real experimental data for use in the dynamic simulation model.

8.1 Initial Test Run

The first test run took place on Nov 19, 2008 with the intention of following the test plan outlined in DR103-03. Disaster struck on the second test point at a pitch angle of -10° and a speed of ~270km/h when the right wing sheared off from the rest of the model and went flying down the tunnel. Testing halted, no useful data for meeting the test objectives was gathered, and the model had to be rebuilt as soon as possible.

This brief test run did however yield some benefits for the team. All interfaces between the model, pitch selector, and fairing were found to be functioning properly, the team members became better aware their roles during the test run, and everyone had a chance to familiarize themselves with the facility. Thus, subsequent test runs were more time efficient and more data could be gathered.

8.2 Model Reconstruction

The first stage of reconstructing the model consisted of an investigation into the causes of the failure. By studying the design and materials from which the model was constructed, as shown in Figure B-26, the following factors emerged as a likely cause of the accident.

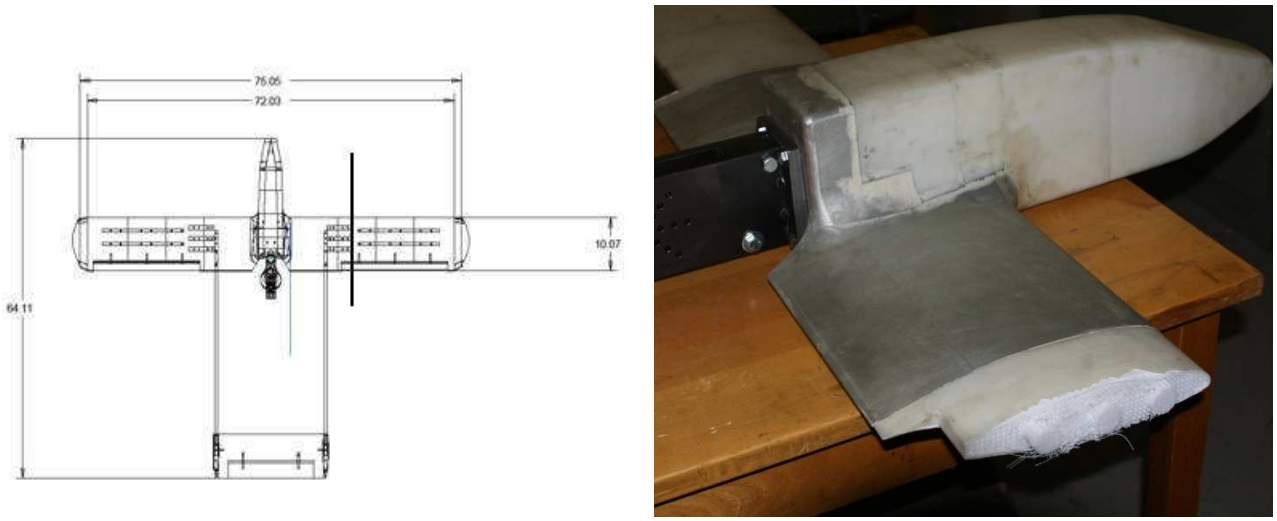

Figure B - 26: Wind tunnel model damage

Most notably the design had a non-continuous wing spar and a sparse plastic-fibre matrix as its core (i.e. it was not solid as intended in the design). Furthermore, the plastic fibres in the outer shell were aligned chordwise along the wingspan and the shell was connected to the spars only on the bottom of the wing. All of these details contributed to weakening a material which already had a theoretically low safety factor to the point where the shell on the top of the wing separated from the inner matrix and subsequently failed under the large bending stresses now imposed upon it due to the lack of a load path to the main spar. Destructive testing of the left wing revealed a similar failure mode at the same spanwise location thus further proving the vulnerability of the design and the validity of the failure mode observed in the wind tunnel.

In rebuilding the model, a design change was made to address the shortcomings identified during the investigation. The wing was built out of a solid piece of oak, with the grain aligned spanwise, which is three times as strong as the plastic and also has a higher Young's Modulus thus bends less under loading. The caps were built out of basswood and fastened to the main wing using two screws. Finally, the wing spars were lengthened and made out of aluminum to better match the stiffness characteristics of the oak. Once the wing was glued onto the aluminum root and spars, two pins were inserted midway along the spar to prevent lateral motion as an added measure of redundancy.

The new model, as seen in Figure B-27, was finished during the second week of January 2009 just in time for the re-scheduled test run on January 23, 2009.

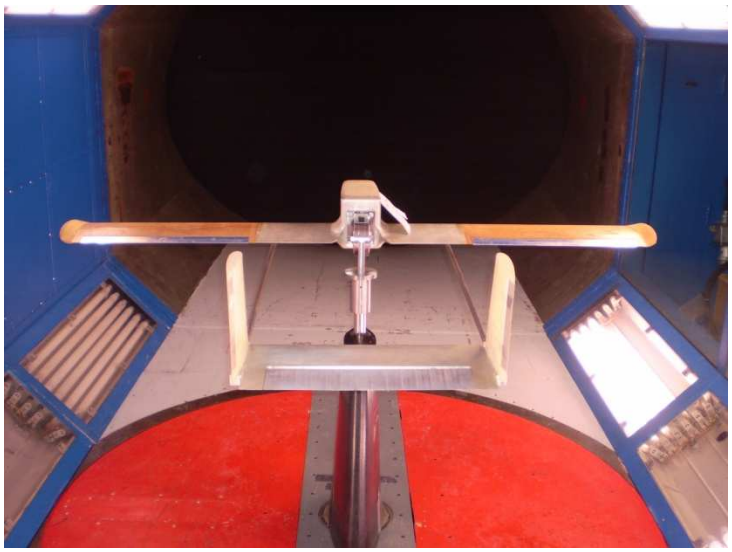

Figure B - 27: Re-built wind tunnel model

8.3 Final Test Run

In order to meet the objectives given the constrained testing timeline it was necessary to adjust the original test plan in such a way that all the data could be gathered in a single day. This was achieved by only running the low speed (64m/s) tests and verifying during one of the tests that the higher speed (105m/s) would yield similar results. No major snags were encountered during this test run thus a complete set of data was obtained for GeoSurv II. The most important results are outlined in the next section.

9. WIND TUNNEL TESTING RESULTS

These results are discussed in detail in DR103-04.

9.1 General Performance

This section of the test plan deals with the overall performance of the aircraft particularly in the longitudinal direction including the drag polar, $C_{L\alpha}$, and $C_{M\alpha}$ curves. Overall, there is good agreement with the analytical and CFD predicted values. Drag measurements fall in between the two predicted solutions thus showing that CFD overestimated the total drag of the aircraft.

9.2 Pitch Stability

This section of the test plan was concerned with the effects of the elevator on the longitudinal stability of the aircraft. Experimental data is in close agreement with CFD estimates; the only problem arises from the fact that theoretical estimates are twice as large as the CFD values. Furthermore, in previous years the elevator was resized based on the theoretical estimates (DR73-12) in order to increase the deflections required for trim. Given now this additional experimentally measured reduction in elevator effectiveness, the performance and required

deflections of the elevator should be closely monitored during flight testing and adjustments made as necessary to maintain performance requirements.

9.3 Directional Stability

This section of the test plan was concerned with the effects of the rudder and sideslip angle on the directional stability of the aircraft. The aircraft was found to be statically stable and at low risk for dynamic instability due to spiral divergence. The two important coefficients in this section, $C_{N\beta}$ and $C_{N\delta r,}$ also define the sideslip envelope of the aircraft. For the GeoSurv II, the maximum sideslip angle was found to be 7.317° thereby reinforcing the need for a steerable nose landing gear as shown in DR73-11.

9.4 Roll Stability

This section of the test plan was concerned with the effects of the aileron on the roll characteristics of the aircraft as well as the effect of flaperons on lift and pitching moment. The experimental values are very close to the analytical predictions and have also been further verified by using the dynamic simulation to show that the roll rate response of the GeoSurv II aircraft is comparable with that of a Cessna 172. The flaperon results were found to be close to analytical predictions thus reinforcing that flaperons are an effective, simple choice for a high-lift device.

9.5 Airbrakes

This section of the test plan was concerned with finding solutions for increasing aircraft drag in order to meet the 10% gradient requirement at cruise. The proposed solution of using rudders as airbrakes was found to increase C_D by 0.013. This is sufficient to meet the descent gradient requirement; however, an updated analysis revealed that using ailerons as spoilers would be a better alternative in terms of implementation difficulty and controllability of the aircraft. This analysis currently does not take into account engine thrust during descent.

9.6 Conclusions

The wind tunnel tests have been performed successfully despite major flaws in the model's initial design which led to a spectacular accident during the first test run. The objectives of the test plan have been achieved: validating analytical and CFD stability estimates, finding a solution for meeting the descent gradient requirement, and gathering experimental data for use in the dynamic model. Achievement of these objectives paves the way for first flight of the prototype.

9.7 Recommendations

- Always plan for a tail-off pitch sweep. More detailed information about the aircraft's performance as well as more accurate wall corrections would be available as a result.

- Replace the vertical stabilizers since the Right (Starboard) one was cracked at the base during the last test run. A test run with the current stabilizers is not advised.

- Descent gradient analysis should be re-visited once engine thrust during descent is known. Implementation of the chosen solution should be discussed with other sub-groups: AVI, STR.

- Closely monitor longitudinal stability and elevator deflections during flight testing to ensure that the resized elevator remains suitable for all phases of flight.

- Verify that the aircraft can meet all crosswind requirements for certification. Most likely through flight testing.

10. TAKE-OFF ANALYSIS

In the previous project year, the elevator was resized from 36% of the tail area to 10%. This was done because analysis with the dynamic simulation showed that the aircraft was extremely sensitive to elevator inputs. With the previous elevator size, the aircraft would have been very difficult to control since very small elevator deflections were required for manoeuvring. More information on this analysis can be found in DR 73-12 and 83-12. During the final elevator sizing this year it came to the attention of the project group that no thorough analysis has yet been completed of the aircraft during take-off conditions. Specifically, an analysis was needed to determine the required elevator size to rotate the aircraft during take-off ground roll since this is imperative for reaching the main project goal of first flight.

10.1 Take-off Moments

For the ground roll section of take-off a moment balance is performed about the main landing gear ground contact point. The largest moments about this point in the pitch-up direction come from the lift due to the wing and the negative lift due to the tail. The largest pitch-down moments are due to the weight of the aircraft and the thrust. For the analysis the elevator size was varied and the speed required for the pitch-up tail moment to overcome the other moments was calculated. The analysis can be found in DR 103-01. A plot of the results can be found below in Figure B - 28.

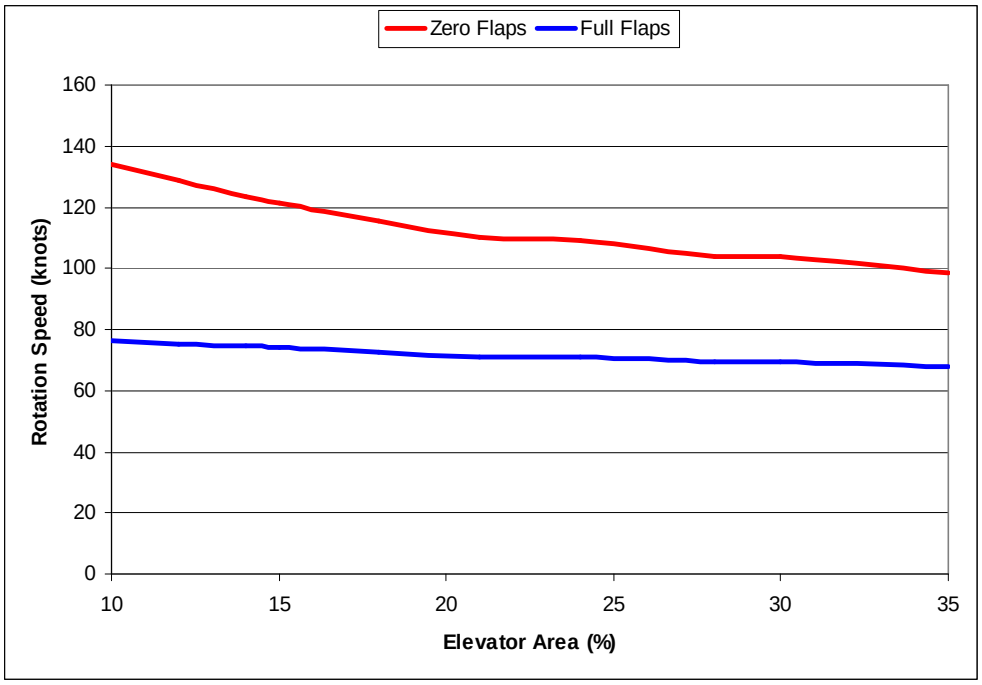

Figure B - 28: Rotation speed vs elevator area

It was found that even with the largest reasonable elevator size and full flap deflection the prototype would not be able to rotate until a speed of almost 68 knots. By this time the lift would have already overcome weight and the aircraft would have lifted off the ground. It would seem that the pitch-down moment due to the thrust is too large to overcome due to the long moment arm. A design change is needed to allow for lift-off at a reasonable speed.

10.2 Landing Gear Design Change

The purpose of rotation is to increase the angle of attack of the aircraft in order to increase the lift coefficient. Since the prototype cannot rotate until a very high speed it is necessary to increase the angle of attack another way. Since wing and tail incidence angles have been optimized for cruise flight the best option is to modify landing gear lengths. For the analysis the angle of attack of the aircraft was varied and the speed at which the lift overcomes aircraft was calculated. The analysis can be found in DR 103-01. A plot of the results can be seen below in Figure B - 29.

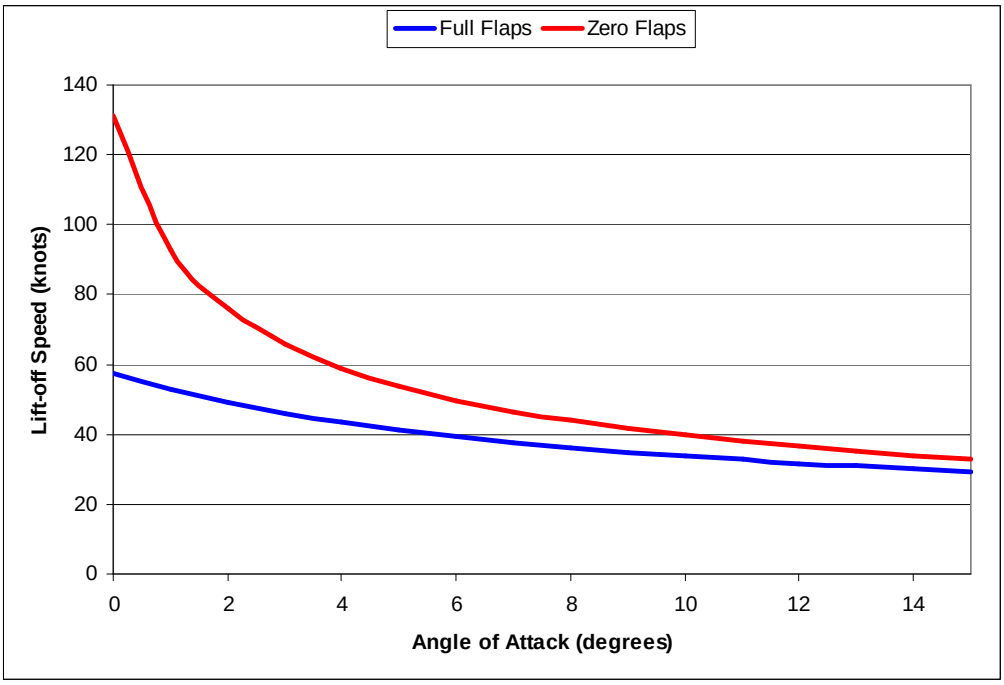

Figure B - 29: Lift-off speed vs angle of attack

It has been suggested by Brian Wattie that the take-off speed be limited to under 50 knots. An increase in the angle of attack of the aircraft on the ground of 4 degrees would reduce the lift-off speed to approximately 43 knots to provide a margin of safety. This would also decrease the ground roll distance from over 1000 ft to under 200 ft. In order to create this angle of attack on the ground the difference between the main and nose landing gears must be 2.5 inches. Discussion with the landing gear team has revealed that the main landing gear as manufactured is 25.5 inches tall; 0.5 inches shorter than the original design drawings. This means that the nose landing gear must be lengthened by 2 inches to a length of 28 inches as shown in Figure B - 30.

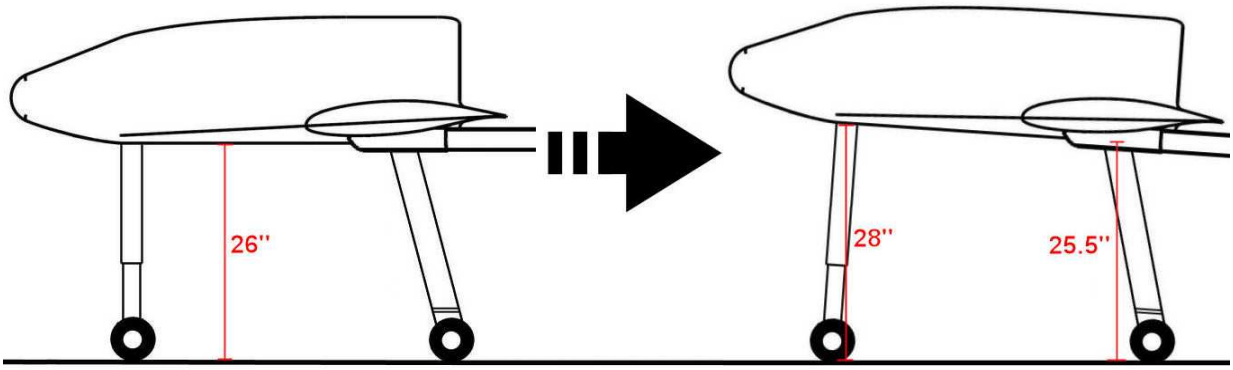

Figure B - 30: Landing gear design change

10.3 Conclusions and Recommendations

- The landing gear must be increased in length by 2 inches in order for a successful take-off at a reasonable speed.

- Because there is no longer any need for rotation, the elevator should remain the 10% tail area size that was determined last year.

11. DYNAMIC SIMULATION

Dynamic simulation is a tool that the design team can use to simulate the flight of the GeoSurv II during the design face. This has a broad range of applications during the design process. It can be used to aid in control surface sizing, it can be used to as a preliminary flight test for pilot testing and training. The model currently in use was developed by Justing Koning and Zhe Yan in previous project years. Koning developed a set of non-linear equations of motion and developed a simulation tool in MATLAB. It can simulate the effect of control surface deflection. It can also be used to test and verify wind tunnel data and compare any discrepancies between theoretical and experimental stability derivatives as well as compare aircraft performance with other aircraft. An example of this is the rolling moment due to aileron deflection. When comparing the theoretical values with wind tunnel data we get Figure B - 31 below.

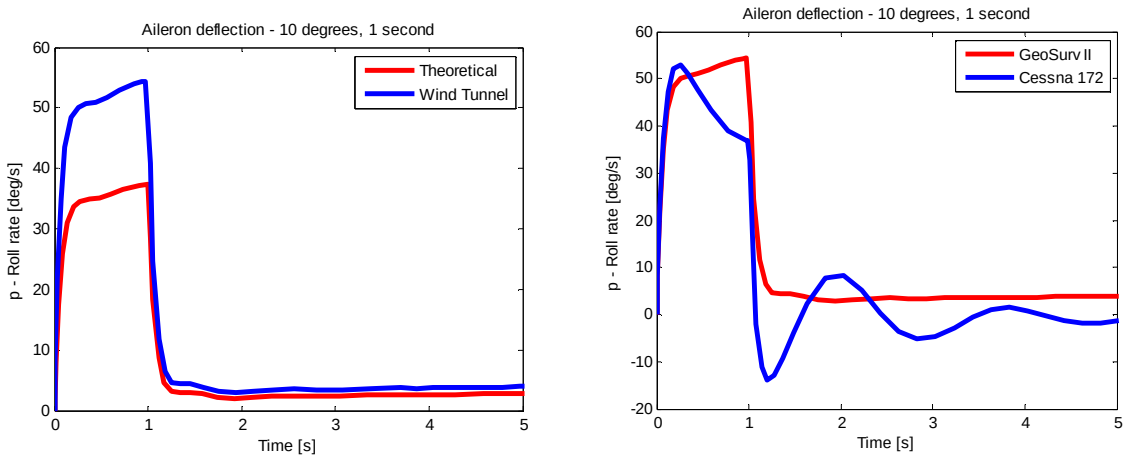

Figure B - 31: Roll rate comparison

Last project year Yan was able to use the linear equations of motion in a Simulink model which takes input in real time and outputs a 3D visualization of the aircraft. The details of his work can be found in DR 83-14.

The linear simulation, however, has limitations. It is only valid for small perturbations. The model can only simulate small control surface deflections and stall cannot be simulated. The goal for this year was to further develop the model into a non-linear model. This would allow much more flexibility. Adverse weather conditions like high winds and gust conditions could be simulated as well as larger control surface deflections.

11.1 Non-linear equations of motion

The first step in developing the non-linear model was to develop the equations of motion that would be programmed into the MATLAB environment. The detailed derivation of the equations of motion in the longitudinal direction can be seen in DR 93-03. A similar derivation was performed for the lateral direction and the resulting equations are:

Translational

$$\dot{u} = \frac{1}{m}\left[L\sin\alpha - D\cos\alpha + T\right] - g\sin\theta + vr - qw$$
$$\dot{v} = \frac{1}{m}\left[Y\cos\beta\right] + g\sin\phi\cos\theta + wp - ur$$
$$\dot{w} = \frac{1}{m}\left[-D\sin\alpha - L\cos\alpha\right] + g\cos\phi\cos\theta + uq - vp$$

where the lift, drag and side-force and non-dimensionalized as:

$$L = C_L \bar{q} S \qquad C_L = C_{L_\alpha}\alpha + C_{L_{\delta e}}\delta e + C_{L_{\delta f}}\delta f$$
$$D = C_D \bar{q} S \qquad C_D = C_{D_0} + C_{D_L}$$
$$Y = C_Y \bar{q} S \qquad C_Y = C_{Y_\beta}\beta + C_{Y_{\delta r}}\delta r + C_{Y_r} r$$

Rotational

$$\dot{p} = \frac{\ell}{I_{xx}} - \frac{\left(I_{zz} - I_{yy}\right)}{I_{xx}} rq$$
$$\dot{q} = \frac{M}{I_{yy}} - \frac{\left(I_{xx} - I_{zz}\right)}{I_{yy}} pr$$
$$\dot{r} = \frac{N}{I_{zz}} - \frac{\left(I_{yy} - I_{xx}\right)}{I_{zz}} pq$$

and the roll, pitch and yaw moments are non-dimensionalized as:

$$\ell = C_\ell \bar{q} S b \qquad C_\ell = C_{\ell_{\delta a}}\delta a + C_{\ell_{\delta r}}\delta r + C_{\ell_\beta}\beta + C_{\ell_r} r + C_{\ell_p} p$$
$$M = C_M \bar{q} S \bar{c} \qquad C_M = C_{M_\alpha}\alpha + C_{M_{\delta e}}\delta e + C_{M_{\delta f}}\delta f + C_{M_q} q$$
$$N = C_N \bar{q} S b \qquad C_N = C_{N_\beta}\beta + C_{N_{\delta r}}\delta r$$

These equations are valid at all times for the aircraft. With these equations the GeoSurv II can be much more accurately modeled over many more flight conditions than was previously possible.

11.2 The Non-linear model

The equations of motion were then programmed into a MATLAB m-file that could be incorporated into a Simulink model. Like the linear model that preceded it, this model accepts inputs from a USB R/C device and outputs a 3D visualization in the Flightgear interface as shown in Figure B - 32. For more analytical purposes scopes can output plots of any parameter one desires. These include:

- Airspeed
- Ground speed
- Altitude
- Longitude and latitude
- Control surface deflections
- Roll, pitch and yaw rates

A more detailed description of the workings of this system can be found in DR 83-14.

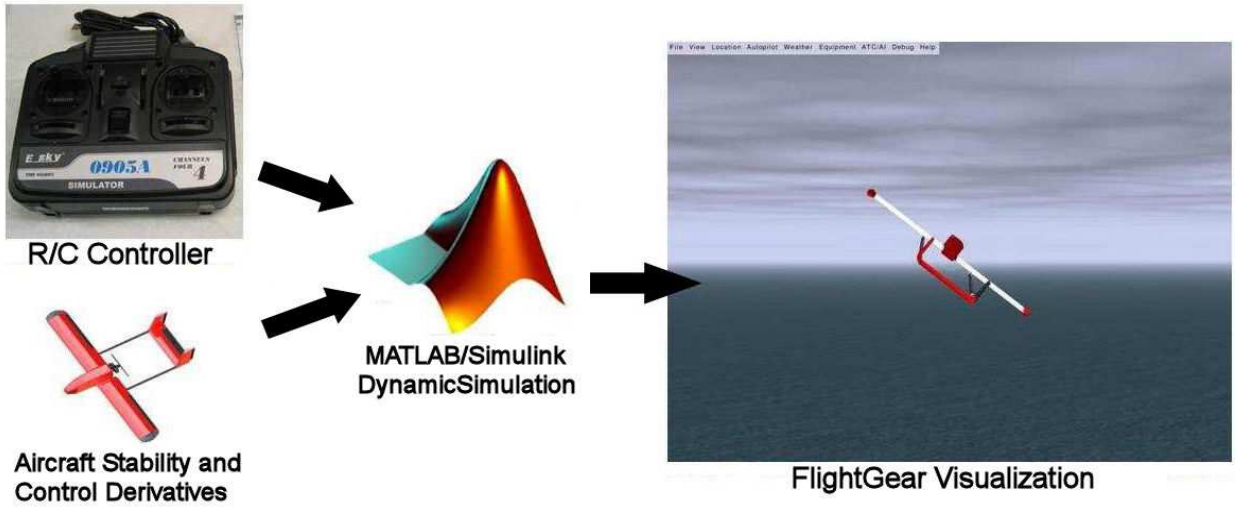

Figure B - 32: Dynamic simulation overview

The main difference between the old linear model and the new non-linear model is the Equations of Motion (EOM) block. The linear EOM block, seen in Figure B - 33, takes inputs of control surface deflections and outputs a forward speed, angle of attack, side-slip, pitch Euler angle, roll, pitch and yaw.

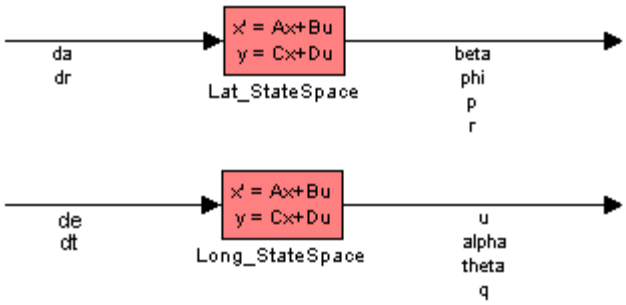

Figure B - 33: Linear equations of motion block

The non-linear EOM block, seen in Figure B - 34, takes inputs of control surfaces as well as the current speed and the orientation of the aircraft in the body and inertial frames. The outputs are the translational accelerations as well as the rotational accelerations in the body and inertial frames.

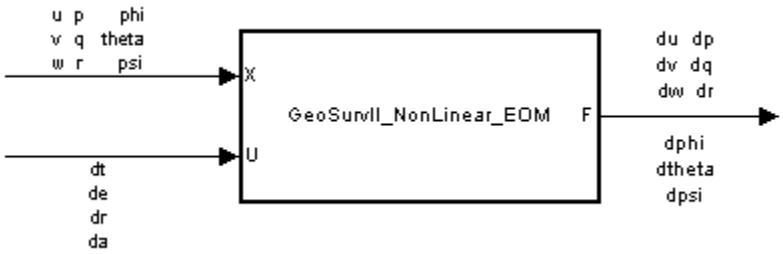

Figure B - 34: Non-linear equations of motion block

This EOM block expresses the non-linear equations in a format that MATLAB can manipulate. The rest of the Simulink model has very similar architecture to the non-linear model. With this it should be possible to compare the aircraft performance to flight data. For a detailed description of the non-linear simulation with instructions on its use, refer to DR 103-07.

11.3 Conclusions and Recommendations

- After flight of the prototype, flight data should be compared to simulation for model validation.
- In addition, simulation of failure modes such as control surface failures should be simulated as well as demonstration of requirements for aircraft certification.
- Work should be done with the avionics group to incorporate the autopilot into the model. This will aid in autopilot refinement and full automated flight testing in a virtual environment.
- GeoSurv II sensors and their respective errors should be incorporated into the model to simulate the ability of the GeoSurv II to follow a pre-programmed flight path relying on sensors for navigation.

ACKNOWLEDGEMENTS

The Aerodynamics and Propulsion group gratefully acknowledges the input and support of the following people:

- Carmelo Scaini (CMC Electronics)
- Alex Proctor (MAE Machine Shop)
- Kevin Sangster (MAE Machine Shop)
- John Bauer (Lead Engineer – Avionics)
- Brian Wattie (Lead Engineer – Avionics)
- Harold Rook (National Research Council)
- Stuart McIlwain (National Research Council)

DESIGN REPORTS

DR 93-01	Concepts for redesign of GeoServ II fuselage to reduce drag, and preliminary CFD simulations	Majed Piedra Abu Sharar
DR 93-02	Air Data Boom Design	Sean Clifford
DR 93-03	Derivation of Equations of Motion in the Longitudinal Direction	Guillaume Blouin
DR 93-04	Engine Test Rig Modifications, Checklist and safety document	Thomas McQueen
DR 93-05	Prototype Fuel System Modifications and Safety Compliance	Thomas McQueen
DR 93-06	Wind Tunnel Model Support System Design and Manufacture, and Test Execution Preparation	Andrei Janus
DR 93-07	CFD	Majed Piedra Abu Sharar

DR 93-08	Final Elevator Sizing	Guillaume Blouin
DR 93-09	Boom design refinement and loads analysis	Sean Clifford
DR 103-01	Take-off Analysis	Guillaume Blouin
DR 103-02	Engine Controls	Thomas McQueen
DR 103-03	Scaled Model NRC Wind Tunnel Test Plan	Andrei Janus
DR 103-04	Scaled Model NRC Wind Tunnel Results	Andrei Janus
DR 103-05	Air Data Boom Manufacturing	Sean Clifford
DR 103-06	Air Data Boom testing	Sean Clifford
DR 103-07	Non-linear Dynamic Simulation Framework	Guillaume Blouin
DR 103-09	Drag Analysis of Nosecone Design and Fuselage Modification	Majed Piedra Abu Sharar